SMART SENSOR AND TRACKING SYSTEM FOR UNDERGROUND MINING

A Thesis Submitted
to the College of Graduate Studies and Research
in Partial Fulfillment of the Requirements
for the Degree of Master of Science
in the Department of Electrical and Computer Engineering
University of Saskatchewan

by

Xuechao Zhang

Saskatoon, Saskatchewan, Canada

Permission to Use

In presenting this thesis in partial fulfillment of the requirements for a Postgraduate degree from the University of Saskatchewan, it is agreed that the Libraries of this University may make it freely available for inspection. Permission for copying of this thesis in any manner, in whole or in part, for scholarly purposes may be granted by the professors who supervised this thesis work or, in their absence, by the Head of the Department of Electrical and Computer Engineering or the Dean of the College of Graduate Studies and Research at the University of Saskatchewan. Any copying, publication, or use of this thesis, or parts thereof, for financial gain without the written permission of the author is strictly prohibited. Proper recognition shall be given to the author and to the University of Saskatchewan in any scholarly use which may be made of any material in this thesis.

Request for permission to copy or to make any other use of material in this thesis in whole or in part should be addressed to:

Head of the Department of Electrical and Computer Engineering
57 Campus Drive
University of Saskatchewan
Saskatoon, Saskatchewan, Canada
S7N 5A9

Acknowledgments

I would like to express my appreciation to my supervisor, Dr. Khan Wahid for his guidance throughout my purchasing this degree. He truly gives many valuable comments and suggestions on my work.

I would also like to thank all my lab mates. They showed great interest in my research and I enjoyed lots of interesting and thoughtful discussions and conversations.

I would like to thank my girl friend, Jing Wang. We have finished our Bechelor's degree and Master's degree together in the same university. She helps me a lot not only in academic life, but also in my personal life.

Finally, I would like to express my thanks to my parents Jian Zhang and Yinxia Ma. Thanks for their support and encouragement for the two years.

Abstract

The thesis predominantly discusses a smart sensor and tracking system for underground mining, as developed by the author. The tracking system is developed by two steps, the first of which involves finding an efficient way to measure the distance, and the second of which involves localizing the positions of each miner in real-time.

For the first step, a Received Signal Strength Indicator (RSSI) is used to measure the distance between two points by indicating the amount of energy lost during the transmission. Due to environmental and human factors, errors exist when using RSSI to measure distance. Three methods are taken to reduce the error: Gaussian distribution, statistical average and preset points. It can be observed that the average error between actual distance and measured distance is only 0.1145 meters using the proposed model.

In regards to the localization, the "3-point localization method" is considered first. With the proposed method, the result of the localization is improved by 0.6 meters, as compared to the "2-point localization method".

The transmission method for the project is then discussed. After comparing several transmission protocols in the market, ZigBee was chosen for the signal transmission. With the Zigbee protocol, up to 65000 nodes can be connected, which are suitable for many miners using the system at the same time. The power supply for the ZigBee protocol is only 1mW for each unit, thus potentially saving a great amount of energy during the transmission.

To render the tracking system more powerful, two smart sensors are installed: an MQ-2 sensor and a temperature sensor. The MQ-2 sensor is used to detect the harmful gas and smoke. In the event that the sensor's detected value is beyond the threshold, it will provide a warning for the supervisor on the ground.

Table of Contents

List of Tables

List of Figures

List of Abbreviations

ADC	Analog-to-Digital Conveter
AHRS	Attitude Heading Reference System
AOA	Angle of Arrival
BLE	Blue-tooth Low Energy
CPU	Central Processing Unit
GPIO	General-Purpose Input/Output
GPS	Global Positioning System
HBE	Human Body Effect
ID	Identity
IMU	Inertial Measurement Unit
MCU	Micro Controller Unit
MSHA	Mine Safety and Health Administration
NFC	Near Field Communication
NIOSH	National Institute for Occupational Safety and Health
PDF	Probability Density Function
QFN	Quad Flat No-lead Package
RFID	Radio Frequency Identification
RSSI	Received Signal Strength Indicator
SFR	Special Function Register
SOC	System-On-Chip
SPI	Serial Peripheral Interface
TI	Texas Instruments
TOA	Time of Arrival
TOF	Time of Flight
UART	Universal Asynchronous Receiver Transmitter
UHF	Ultra High Frequency
USART	Universal Synchronous/Asynchronous Receiver/Transmitter

1. Introduction

1.1 Background

Coal mines are undoubtedly a precious wealth of nature. Many countries devote copious amounts of effort into the mine industry for the purpose of driving economic growth. However, as a result of natural factors, human errors, unreliable technologies, and other circumstances, mining accidents never cease to occur. This is especially true of developing countries, which without strict operation rules, qualified laborors and advanced technologies, experience fatal coal mine accidents nearly every year [11].

A significant amount of miners lose their lives as a result of mining accidents every year. The Chinese mine industry is a prime example. According to the National coal-mining safety accident report in China 2014-2015 [12], there were 26 reported mining accidents and 167 deaths of miners in 2015. The largest accident took a devastating 22 lives. In 2014, 252 people died in 48 mining accidents. The statistics in Table 1.1 reveal that, before 2008, over one thousand miners lost their lives every year.

In the developed countries such as the United States, the miners also work in an unsafe environment. Figure 1.1 reveals the statistics obtained from the Mine Safety and Health Administration (MSHA). It discloses the number of deaths from 1969 to 2014 in the USA. From Figure 1.1, it can be observed that 16 miners died in 2014 as a result of coal mine accidents, while 260 miners died in 1970. The death of miners in America raised people's attention. Furthermore, in 1969, miners started to fight for their rights and ensure that the law protect their safety and health. Although the law [14] may decrease the number of

Table 1.1 Number of deaths in coal mining accidents in China, 2001-2008

Year	2001	2002	2003	2004	2005	2006	2007	2008
Deaths	2613	4251	4899	3603	3925	1673	1368	1086

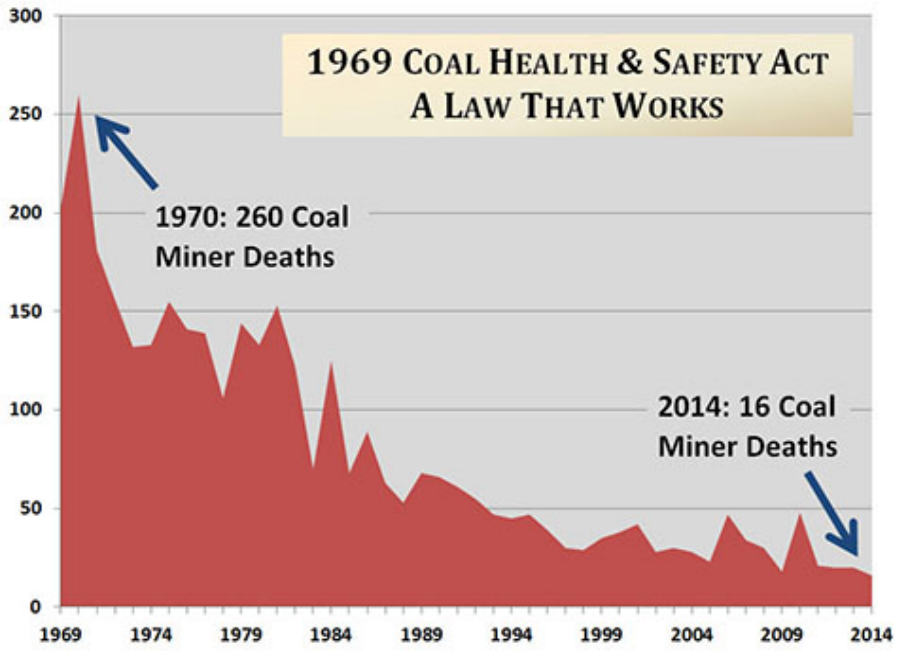

Figure 1.1 The number of coal miner deaths in USA, 1969-2014 [13]

deaths, it fails to eradicate the occurrence of mine accidents. The miners' safety issues are long-standing and elicit concern worldwide [15].

The mine industry is also one of the most indispensable and lucrative industries in Saskatchewan. It is the largest potash [16] producer in the world, generating a handsome revenue of 8.5 million tones per year. Moreover, Saskatchewan ranks the third largest producer of coal in Canada, which outputs 11.6 million tones per year. Therefore, in Saskatchewan, the safety of miners is an essential matter. The relevant miner tracking systems have already been applied to mines in Saskatchewan, with the objective of tracking and protecting the miners.

1.2 Literature Review

A significant amount of miners worldwide lose their lives every year during the underground. The shocking death statistics have propelled the development of technologies to help guarantee the safety of miners. A portion of the existing localization methods are introduced in this section.

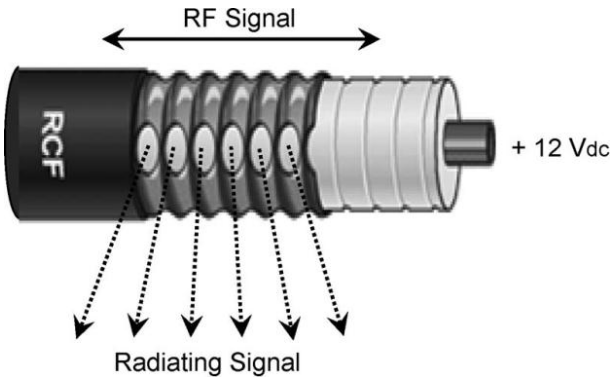

Figure 1.2 Leaky-Feeder Cable [3]

1.2.1 Underground Communication System

Many companies make localization systems. The company Tallysman Wireless designed a reliable tracking system called TagLocate System, which enables the supervisor on the ground to know the positions of all underground people.

The system uses Leaky-feeder and Radio Frequency Identification (RFID) to achieve the communication. The Leaky-feeder has been used for routine communications for more than 35 years. The leaky-feeder system has a dual role of both a communication line and distribution antenna. As depicted in Figure 1.2, the radiating signal can get into and out-of the leaky-feeder cable. Therefore, the system can easily achieve the two-way communication.

Normally, the leaky-feeder system works at a high working frequency, from 30 MHz to 300 MHz. The enhanced frequency can be up to 450 MHz, which is in a Ultra High Frequency (UHF) band (300-3000MHz). The high frequency and large bandwidth results in high signal transmission rates. The signal in UHF additionally provides more optimal propagation characteristics in free space [17]. However, a more expensive cable is required as a result of the higher frequency and wider bandwidth. Higher line attenuation and coupling loss will also occur in this situation.

The basic operation system is displayed in Figure 1.3. From Figure 1.3, it can be observed that the base station is on the ground and it controls all communication systems. The shaft, which cannot radiate, connects the base station with the Leaky-Feeder cable. The cable extends completely around the mine. The handset is a tool with the ability to transmit signals to the cable and receive signal from the miners. In order to call the other miners,

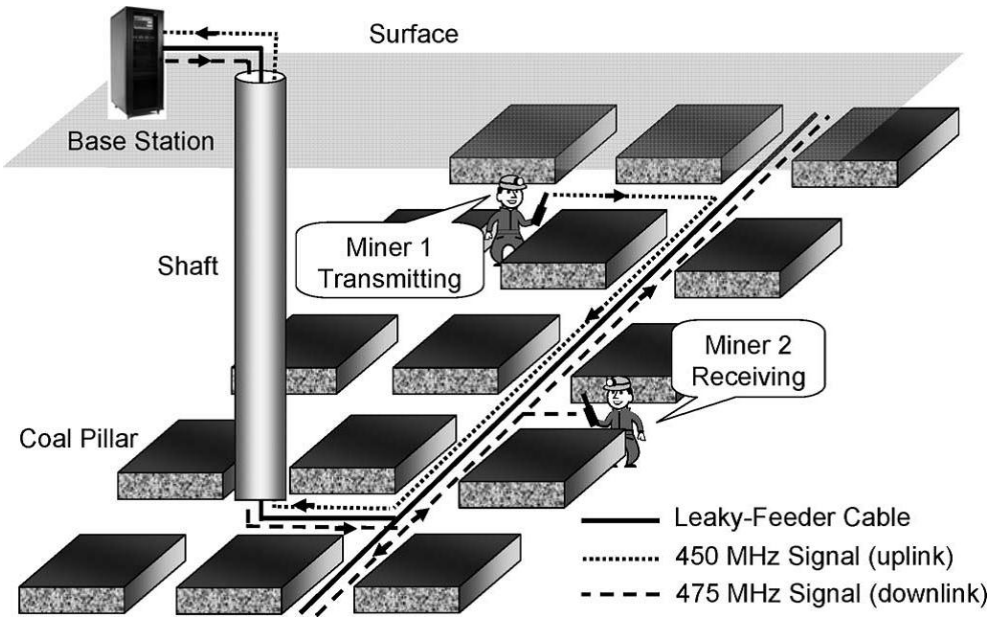

Figure 1.3 Operation System for Leaky-Feeder Cable [4]

the caller must move to the vicinity of the cable.

In order to enable two-way communication for both transmitting and receiving frequencies, the leaky-feeder uses an analog format with frequency modulation for the voice communication. As can be discerned from Figure 1.3, the signal will be transmitted from the Miner 1 at 450 MHz. The signal at this frequency will be only amplified in the uplink direction. After the base station receives the signal, it returns the signal back at 475 MHz. The amplifier in the cable will transmit the signal in the downlink direction from the base station. Finally, the Miner 2 will receive the signal. Up to sixteen different channels can be used for the communication at the same time. Different channels can be employed for different uses. For example, some channels are used for construction and maintenance.

In the Leaky-Feeder system, the tracking system is separated. Usually, the radio frequency identification (RFID) is an easy method by which to track. The active RFID tracking system includes electronic readers and tags. The tag usually plays the role of both transmitter and receiver, and is placed on the miner's hat or in their clothes. Each tag has its own unique ID. The electronic reader is always installed at a stable location, along with the mine, with its own location identification. In the system, the reader can transmit a signal in all directions to ask for feedback from the tag. If the tag is in the coverage of the reader

and it catches the signal, the tag will send back a signal with its own identification code to the transmitter. In addition, the signal also carries the information of the miner. After getting the signal from the miner, the reader will transmit its location code and the miner's information to the ground control center using the leaky-feeder cable. The control center will get a zone-based location because the reader does not give the distance between the reader and tag. In order to obtain a more accurate location of the miner, systems need to be developed to analyze the received signal strength indicator (RSSI) in order to detect the distance and direction between the reader and miner.

The Leaky-Feeder system has many advantages. The technology has been used for a significant amount time and many miners and operators have become accustomed to it. The system has already received approval from the NIOSH (National Institute for Occupational Safety and Health), thereby rendering it reliable. For this system, only a few power supplies are needed. The batteries can be utilized as a backup when the power supply fails to work properly. Furthermore, in the event of an accident, the rescue team merely needs to fix a small amount of power points, after which the system can restart and resume normal functioning.

The Leaky-Feeder cable system also has some disadvantages. The main disadvantage is that the cable must be installed along with the mine continuously, rendering it difficult to cover the entire area. Considering the fact that the mining company is usually developing a new tunnel, the installation and maintenance of the system proves to be a problem. Moreover, the system is only feasible for communication among the miners and cannot do the tracking. The extra system is required if the base station wants to know the location of miners.

1.2.2 Smart Sensor and Tracking System

Some tracking products in the market are introduced and compared in Table 1.2 and 1.3,

A company called X-IO Technologies uses the Inertial Measurement Unit (IMU) and Attitude Heading Reference System (AHRS) to detect the human body motion to obtain the path of the human. The main objective of this tracking method is to detect the motion of the human body and, subsequently, use the computer to simulate the path of the human. The system uses a sensor call MPU 9150 [22], as displayed in Figure 1.4.

The sensor is a 9 Degrees of freedom breakout. It contains an accelerometer, gyroscope

Table 1.2 The comparisons between some tracking products in the market I

Product name	Technology	Ability
AeroScout [18]	Wi-Fi RFID visibility solution. With tags and mobile view included.	1. Real-time visibility 2. Employee visibility 3. Distress alerting, for example detecting the gases: H_2S, O_2, LEL, CO, SO_2, NO_2 4. Ore production visibility 5. Asset visibility
iBeacons [19]	Bluetooth is low power consumption. It can be applied in IOS or Android devices.	An app based on iBeacons can be used to estimate your proximate location and then adjust its behavior based on the iBeacons. It is often applied in: 1. Education 2. Dating 3. Home Electronics 4. Events and Sports.

Table 1.3 The comparisons between some tracking products in the market II

Product name	Technology	Ability
Minetec (SMARTS) [20]	Combining optic fibre, Ethernet over Leaky Feeder (ELF), and WiFi solutions that are designed specifically for Underground deployment.	1. Long-term simulation and cost productivity, modeling 2. Real-time adaptive optimization 3. Real-time traffic management and high accuracy situational awareness
Miniaturized radar and IMU under the shoes [21]	Footsteps can be measured by wearable sensors to determine miners' underground locations	GPS is not needed.

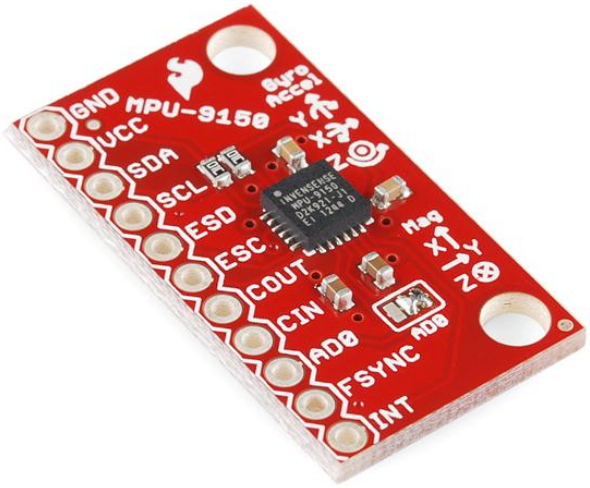

Figure 1.4 MPU 9150

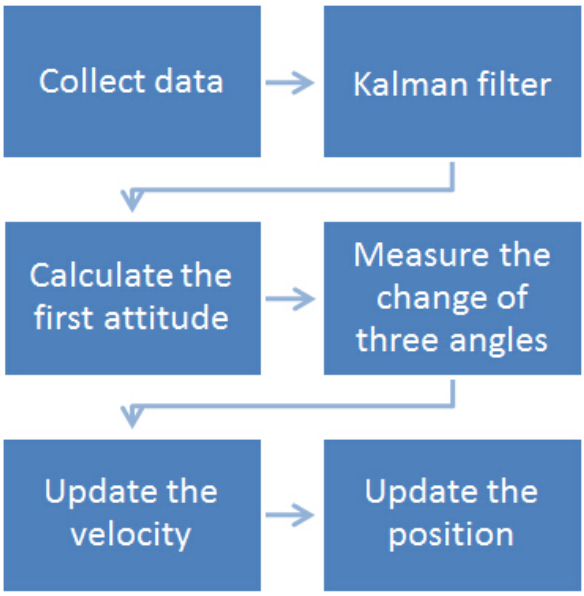

Figure 1.5 The working progress of the tracking method using MPU 9150

and magnetometer. It is also the first 9-axis Motion Tracking Device that is low-cost, high-performance, and has minimal power consumption. The working progress of this method can be observed in Figure 1.5.

The sensor is able to detect the change of angle and acceleration in three dimensions. Using these changes, the position and the walking distance can be calculated using the mathematical algorithm. The example result is displayed in Figure 1.6.

The advantage of this product is that the path of the miner can be detected accurately. However, the disadvantage is that the path cannot be transmitted to the central computer in the real-time. The user should collect all of the data after using the sensor. Even a small adjustment to the data during data collection will result in the whole path being changed.

1.3 Problem Statement

Currently, many products have been developed that are able to track the positions of the underground miners. However, each product has its own disadvantages, most of which are expensive. In regards to the small mine companies, most do not want to spend a large sum of money to buy an entire tracking system. Moreover, most of the existing tracking systems are not powerful enough to detect and report danger in real time or even ahead of time. Taking into consideration the drawbacks of the existed systems, this project aims to

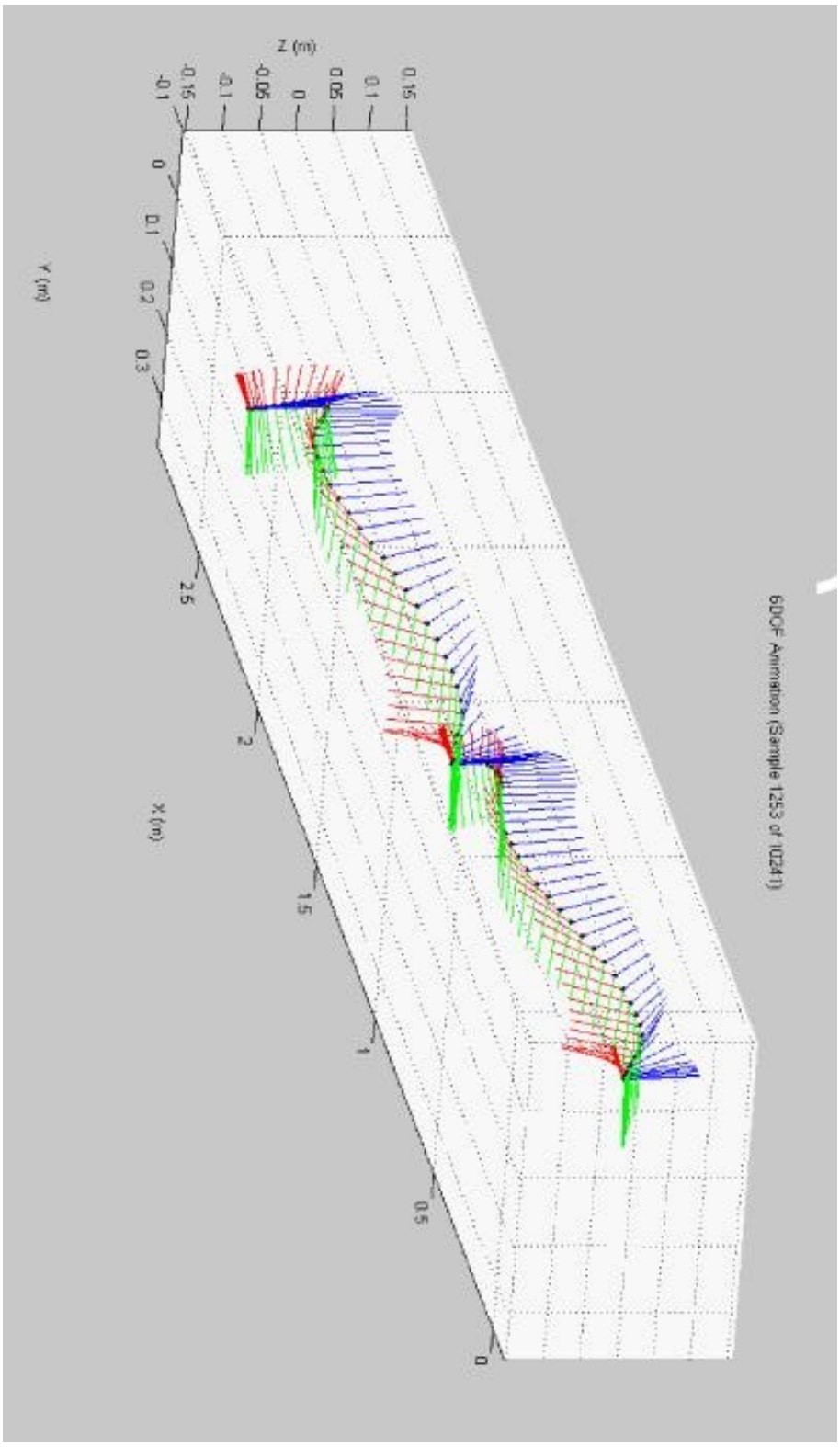

Figure 1.6 An example result of the IMU [5]

Table 1.4 The percentages of deaths by type of coal mining accident in China, 2001 - 2008

Year	2001	2002	2003	2004	2005	2006	2007	2008	Ave
Gas explosion	47.7	31.4	27.7	31.1	38.5	39.1	36.4	26.8	34.2
Collapse	19.7	28.5	31.9	34.4	26.2	16.9	14.9	11.8	26.4
Gas outburst	13.9	15.1	17.0	13.0	10.4	20.9	22.6	34.4	16.0
Water leakage	12.0	10.5	10.4	9.3	13.2	14.3	17.0	16.9	11.9
Machinery	5.4	8.4	11.8	10.5	9.6	5.0	3.7	2.9	8.5
Fire	1.3	6.1	1.2	1.7	2.1	3.8	5.4	7.2	3.0

develop a cheap and multifunctional tracking system.

1.3.1 The Expected Functions of the Tracking System

To avoid mine accidents, the factors that precipitate deaths of the miners should be analyzed first. Table 1.4 [23] lists various factors that have resulted in deaths of the miners from 2001 to 2008.

It is depicted in Table 1.4 that the predominant life threatening hazards are gas explosion, collapse, gas outburst, water leakage, machinery and fire. Therefore, the miners' safety protection system ought to be multifunctional in order to avoid as many life threatening hazards as possible.

From Table 1.4, it can be deduced that more deaths resulted from a gas explosion than any of the other hazards, with a mean percentage of 34.2% over the course of eight years. The gas outburst ranks third place, which also causes 16% of the accidents. Unfortunately, the percentage of deaths caused by gas outbursts continues to increase in incidence. In the recorded eight years, over half of the mine accidents were caused by gas, which will be an increasingly significant problem for miners in the future. Therefore, this tracking system is indispensable to the safety of miners, and will thus help in reducing the incidence of mining accidents in the future.

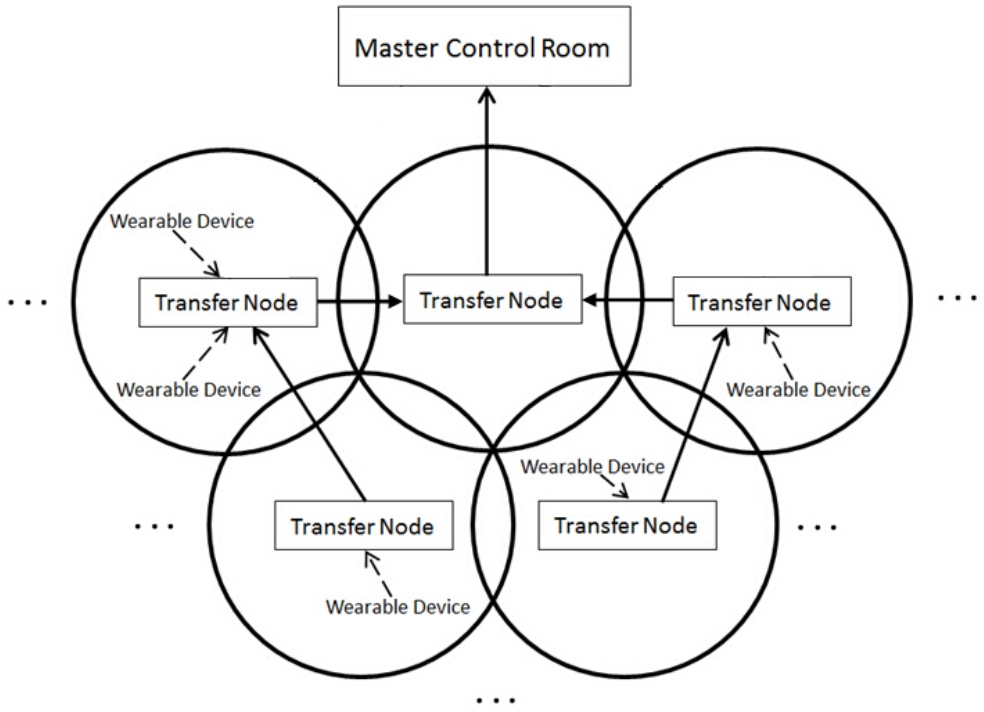

Figure 1.7 The hierarchy relationship between the wearable devices, transfer nodes and the master control room

In reference to Table 1.4, collapse ranks the second most prominent of all death types of mine accidents over eight years, causing 26.4% of deaths. In the years of 2003 and 2004, collapse even became the first killer. Collapse is very difficult to detect ahead of time. Therefore, once it occurs, the ability to save miners' lives is determined by the ability to know the precise position of every buried miner. With this information, the rescuers can rescue the buried miners directly without wasting time digging extensively to find them. In this manner, the injured miners will be able to get medical treat as soon as possible. The buried miners are able to get oxygen, water or even food during the rescue. All this can be achieved with the help of a precise localization system.

1.3.2 Structure of the Smart Tracking System

The improved tracking system contains three main components: wearable devices, transfer nodes and a master control room. The hierarchy relationship between them is delineated in Figure 1.7.

Anyone who enters the mine, including visitors, must put on a wearable device. The

wearable device can help with localization, along with monitoring the nearby environment. If a danger is detected, the wearable device is designed to deliver a warning to the miner and also report to the master control room. This allows the minor to retreat from the dangerous place as soon as possible. For example, if a wearable device detects that the concentration of carbonic oxide in the air is too high, it will beep and warn the miner to leave. At the same time, the message will be sent to the master control room. Once those on the ground get the warning message, they can inform all underground miners to take proper action.

The transfer nodes will be installed on the wall of the mine tunnels and the signal of the transfer nodes will cover the entire underground activity area. These transfer nodes can help to localize the position of each wearable device, allowing the master room to have the real-time position of every miner. The transfer node has the additional function of data transmission. The wearable device will send the data package to the nearest transfer node. The transfer node will go on passing the data package in the direction of the master control room. Moreover, the transfer nodes are able to monitor the environment independently and report to the master control room or warn the around wearable devices directly.

The master control room is responsible for processing the data of all miners and the environmental data. In the event of a reported warning, the master control room should inform every miner and arrange repairing, which will prevent accidents from happening. Once there is an accident, the master control room can quickly determine the positions of all trapped miners, saving crucial time for life searching.

The whole system offers three types of services: precise localization, environmental monitoring and assessment, and body condition monitoring. The rationale for developing and improving functions in these three fields are explained in the following three subsections.

1.4 Thesis Outline

This thesis is comprised of six chapters.

The first chapter introduces the background of the project. As a result of the booming of the mine industry and the serious lack of adequate protection technologies, the development of an affordable and smart real-time tracking system is an indispensable endeavour. Although there are presently underground communication systems, underground tracking systems and

localization systems in the market that are seemingly effective, each of these have their own disadvantages. With the knowledge of the current technologies, a real-time tracking system with functions such as harmful gas monitoring is expected to be developed. The structure of the tracking system consists of three parts: the wearable device that localizes and monitors the environment around the wearer, the transfer nodes that are installed on the wall and can monitor the surrounding environment and help data transmission, and the master control room that has a central computer to process all collected data and allows supervisors to send out messages in accordance with different situations.

In the second chapter, an algorithm for distance measurement based on ZigBee is introduced. The algorithm is used for the underground mining tracking system. At the first step of the algorithm, the Gaussian distribution function is applied to avoid large effects and low possibility events. Then, the statistical average is calculated for the more accurate data. Finally, three checking points are set to reduce the interference from the environment to the human body. The RSSI in one-meter transmission, the signal propagation and human body effects are measured by the checking points. These parameters can be updated in the central computer in real time. Several experiments are conducted using this model, with the average difference between the actual distance and calculated one being only 0.1145 meters. The results demonstrate that the model works well. However, improvements to the algorithm could still be made. In the future, more effort will be devoted to decreasing the interference from barrier.

Chapter 3 predominantly discusses the transmission method for this project. The ZigBee protocol is used because of its advantages. The device can connect to a maximum of 65000 nodes, which is suitable for many miners using the device at the same time. Moreover, the power supply is only 1mW for each unit, which has the potential to save a great deal of energy during transmission. In the underground transmission system, the transfer nodes act as transmitters. Transfer nodes receive the data package from wearable devices and transmit the data to the master control room. There are two situations for which this method is employed. One is in the event that the wearable device sends out a data package. In this case, the nearest transfer node will measure the RSSI and create a new package that includes data from the wearable device. The new data package is then transferred to the previous

transfer node. The other case is that some transfer nodes send out a data package. This transfer node will merely transfer the entire data package to the previous node. Using this method, the miner does not require a cable to connect transfer nodes. In the final transfer node, a data connection is installed, which is able to collect the data from the transfer node and transfer it to the central computer using a serial cable. Finally, the supervisor on the ground can track each miner underground and detect regions of danger.

The fourth chapter introduces the localization method of the tracking system. Usually, a point can be precisely localized with three points (the 3-point localization method). However, when taking into consideration the particularity of the mine tunnel, it is found that two points are sufficient for positioning a point in a mine tunnel. If one were to regard the two reference points as circle centre and the measured distances from the two reference points to the miner as the radius, two circles can be drawn and two cross point occurs. Only the cross point located in the tunnel could be the position of the miner. Therefore, when a miner wears the wearable device, the nearest two transfer nodes can localize the position of the miner. This method is referred to as the '2-point localization method'. In order to improve accuracy, the nearest three transfer nodes are used for localization. Each two nodes comprise a pair and the '2-point localization method' can be applied for localization. Three different positions will be measured with these three pairs of nodes. The average of these three will be determined as the position of the miner. With the improved method, precision of localization is improved by 0.6 meters, as compared to the '2-point localization method'. In comparison to the existing localization method, this improved method demonstrates superior performance.

Chapter 5 introduces the CC2530 development board and sensors used in the system. Two analog sensors are installed in the device: a temperature sensor and an MQ-2 sensor. The temperature sensor can detect the temperature of the environment. The MQ-2 sensor can detect harmful gases and smoke in the environment. The threshold values for both gases are set according to the experiments. If the measured value is higher than the threshold value, the area is considered dangerous.

Chapter 6 provides a summary of the project. The system performs well under testing conditions, but a considerable amount of work is still required before it can be made into a

product. Future directions for research are included in this chapter.

1.5 Research Objectives

The developed smart tracking system is expected to achieve the following objectives:

- Develop an algorithm for precise distance measurement based on the Zigbee protocol.
- Develop a precise localization method to achieve real-time tracking.
- Monitor and assess the environment around each miner and in the working places. Special attention should be devoted to harmful gases and smoke.
- Make the system easy for installation, expansion and re-planning.
- Ensure the system has low power consumption and is affordable.

2. Distance Measurement Using RSSI

2.1 Received Signal Strength Indicator (RSSI)

There are three main methods measuring the indoor wireless distance: Time of Arrival (TOA [24]), Angle of Arrival (AOA [25]) and Received Signal Strength Indicator (RSSI) [26]. Table 2.1 summarizes the key parameters, advantages and disadvantages of these three methods.

TOA is also referred to as Time of Flight (TOF). This method measures the distance based on the time duration of the signal transmitting from the transmitter to the received. The distance can be calculated by multiplying the time and the speed of light. This technology requires a highly sensitive sensor in order to detect the time of arrival. The TOA is widely used in radio location systems, such as GPS [27].

AOA is a technology that measures the distance based on the angle of arrival. The AOA requires the sensor to detect the arrival angle of the signal from the unknown transmitter. The AOA and TOA have a high requirement for the sensors and also require a complex calculation.

The Receiver Signal Strength Indicator (RSSI) is a measuring method which is dependant upon the strength of the received signal. The most important application of the RSSI is to monitor the reverse interference in telecommunications companies. For a mobile phone user, the unusual RSSI will affect the quality of communication. Normally, the value of the RSSI is between -93 dB and -113 dB. If the value is out of this range, the customer will experience a suboptimal quality of the call, experience difficulty joining the call, or may even be unable to make the call.

There are three unusual conditions for RSSI: too low, too high and changing too much. Table 2.2 depicts these different phenomenons and the possible reasons for these three dif-

Table 2.1 Comparisons between different distance measurement methods

	Full Name	**Key Parameters**	**Advantages**	**Disadvantages**
TOA	Time of Arrival	Time	Different environment don't affect the result.	Need high sensitive sensor.
AOA	Angle of Arrival	Angle	Different environment don't affect the result.	Need high sensitive sensor.
RSSI	Received Signal Strength Indicator	Transmitted power,signal propagation.	Easy to be detected.	Environment affects the result.

Table 2.2 Three conditions for unusual RSSI

RSSI Problem	**Phenomenon**	**Possible Reasons**
RSSI too low	RSSI is always lower than -113dBm, it does not change with the change of power supply.	1. Quality of the product: Connection between the antenna and circuit does not work. 2. The hardware is not reliable. 3. Power supply has problems.
RSSI too high	RSSI is always higher than -93 dBm, or the RSSI is higher than -93dBm in the certain time.	1. ABIS and FMR is not enough due to too many phone working at the same time. 2. The parameters in the system are set incorrectly. 3. Some interference.
RSSI changes too much	The change is more than 6dBm every time.	1.Quality of the product. 2.Outside interference.

ferent RSSI problems. From Table 2.2, it can be deduced that the majority of unusual RSSI conditions are a result of product quality and outside interference. Considering the fact that the RSSI can detect reverse interference, the carrier can determine the reverse interference based on the amount of RSSI.

The RSSI [28] can be used to measure the distance from the transmitter to the receiver [29]. As we know, the power of the signal reduces during transmission; if the amount of power consumed in transmitting a certain distance is known, it can then be used to measure the other transmission distances. This can be achieved by comparing the reference distance to the reference power and then multiplying it by the received signal power.

If the reference distance is denoted 'd_0', the received power measured at the reference distance is denoted '$P_r(d_0)$' in dBm, the distance to be measured is denoted 'd' and the signal power measured at the receiver (which is d meters away from the transmitter) is $P_r(d)$ in dBm, the computation equation is given by:

$$P_r(d)(dBm) = P_r(d_0)(dBm) - 10lg\frac{d}{d_0}; \tag{2.1}$$

The signal transmission can be affected by the environment, interference and the transmitted power. Taken these factors into consideration, Equation 2.1 can be modified as:

$$P_r(d)(dBm) = P_r(d_0)(dBm) - 10nlg\frac{d}{d_0} + X(dBm); \tag{2.2}$$

where $X(dBm)$ is a Gaussian distribution variable whose average is 0 and n is a signal propagation constant which is related to the environment.

Equation 2.2 is a Shadowing Model, which can be used to reveal the relationship between the RSSI and distance. In practical application, the Gaussian noise can be ignored. Equation 2.2 can be simplified as:

$$P_r(d)(\mathrm{dBm}) = \mathrm{P_r(d_0)(dBm)} - 10\mathrm{nlg}\frac{\mathrm{d}}{\mathrm{d_0}}; \tag{2.3}$$

If the reference distance is set to be 1 meter ($d_0 = 1$), Equation 2.3 can be rewritten as:

$$RSSI(\mathrm{dBm}) = \mathrm{A} - 10\mathrm{nlg(d)}. \tag{2.4}$$

where variable A refers to the power consumption (dBm) for 1 meter signal transmission.

The distance can now be measured with the RSSI using Equation 2.4. However, there are several problems that may affect the accuracy of the results in underground mining [29]:

- The signal propagation (n) will change when the environment has changed.
- 'A' will float with a different 'n'.
- The miners wear the carriers on their bodies or in their pockets at different heights. The position of the carrier and height of different people may affect the value of the RSSI, as anything between the transmitter and receiver will alter the RSSI. This effect is referred to as the human body effect (HBE).
- Some events with low possibilities, yet large interferences, may exist. These events will result in a considerable discrepancy between the measured RSSI and the real value.
- The tunnel is narrow and, thus, there are many reflections in the walls. These reflections will alter the results.

As a result of these types of interference, a 3-step model [30] is built to decrease the noise.

2.2 Proposed Algorithm

2.2.1 Step 1: Filter the Small Possibility Event Using Gaussian Distribution

During the measurement, the receiver will be sent many different values of RSSI in one position. As a result of the interferences, although certain events may have a low possibility of occurrence, they exert large effects on the result. For example, the value may suddenly drop as a result of obstruction. This type of value decreases the accuracy of the results. Gaussian distribution [31], also known as normal distribution, has the ability to help to pick up the RSSI in a high possibility area. After the selection, localization accuracy can be improved [32].

Gaussian Distribution

The Gaussian distribution is usually called Normal distribution, which is widely used in statistics, signal processing and image processing. Gaussian distribution depicts a continuous possibility function. When a set of random variable X follows a possibility distribution which has μ and σ, it can be written as:

$$X \sim N(\mu, \sigma^2); \tag{2.5}$$

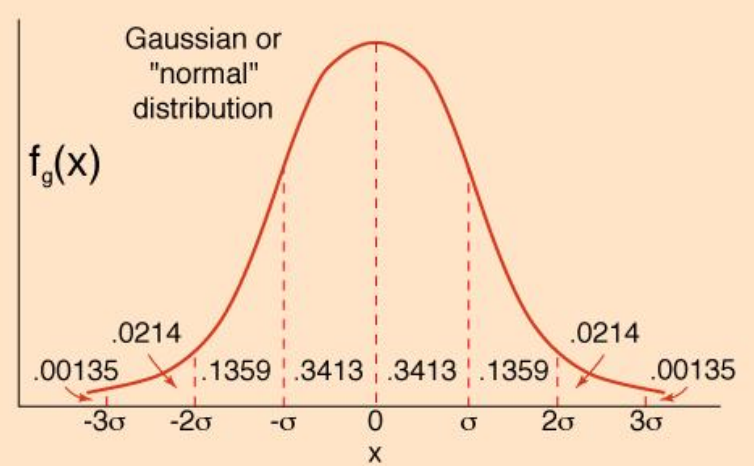

Figure 2.1 Gaussian Distribution [6]

where μ denotes the mean or the expectation, which will determine the position of the distribution. It can be derived as follows:

$$\mu = \frac{1}{n}\sum_{i=1}^{n} X_i; \tag{2.6}$$

σ denotes the standard deviation, which will determine the scope of the distribution. It can be derived as follows:

$$\sigma^2 = \frac{1}{n-1}\sum_{i=1}^{n}(X_i - \mu)^2; \tag{2.7}$$

The probability density function (PDF) is derived as follows:

$$F(x) = \frac{1}{\sigma\sqrt{2\pi}} e^{\frac{-(x-\mu)^2}{2\sigma^2}}; \tag{2.8}$$

where $F(x)$ is the probability density distribution.

When one refers to the standard Gaussian (Normal) distribution, this translates to μ=0 and σ^2=1. The distribution function can be rewritten as:

$$F(x) = \frac{1}{\sqrt{2\pi}} e^{\frac{-x^2}{2}}; \tag{2.9}$$

The plot of the standard Gaussian distribution is depicted in Figure 2.1.

From Figure 2.1, it can be deduced that:

- 68.26% of the area is within [$-\sigma$,σ];
- 95.44% of the area is within [-2σ,2σ];

- 99.73% of the area is within $[-3\sigma,3\sigma]$;
- 99.99% of the area is within $[-4\sigma,4\sigma]$.

Using the Gaussian distribution feature, we can filter the low possibility events in the measurement to improve the accuracy. As per the practical experience, 0.7 is selected as the critical point of the Gaussian distribution. The formula can be written as:

$$0.7 < F(x) = \frac{1}{\sigma\sqrt{2\pi}} e^{\frac{-(x-\mu)^2}{2\sigma^2}} < 1. \tag{2.10}$$

From Equation 2.10, it can be observed that if the value of $F(x)$ is higher than 0.7 and less than 1, the RSSI is considered to be a high possibility value. If the value of the $F(x)$ is lower than 0.7, the RSSI will be considered a low possibility value. The low possibility RSSI value can then be filtered by the Gaussian distribution. Subsequently, the RSSI values which are in the range of Equation 2.10 can be selected and saved in an array known as '$Gaussian_rssi$'.

However, the Gaussian distribution function is only able to reduce the interference with a low possibility and a large effect. It cannot resolve other problems.

2.2.2 Step 2: Statistical Average

When conducting an experiment, there must also be some differences between the real values and the measured values. If we merely choose a single measured value to be the result, the result will be unstable. The uncontrollable factors cannot be changed or ignored. To obtain a better result, we can collect a large quantity of data with the same experimental conditions and calculate the statistical average of the data. With this process, the redundancy will be removed and the accuracy will be improved.

Statistical averaging is a method which calculates the mean of a set of RSSI values from the same receiver. In the first step, the processed RSSI values are save in $Gaussian_rssi$. Therefore, the statistical average can be easily calculated by:

$$Average_{rssi} = \frac{1}{n} \sum_{i=1}^{n} Gaussian_{rssi}[i]. \tag{2.11}$$

With the addition of Step 2, the accuracy can be improved.

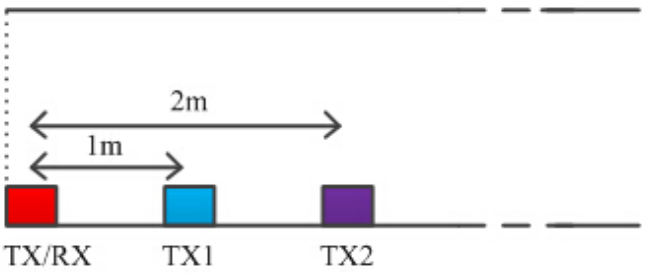

Figure 2.2 Checking point 1 and 2

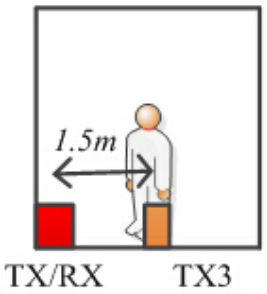

Figure 2.3 Checking point 3

2.2.3 Step 3: Preset Point to Measure the 'n', 'A' and HBE

From Equation 2.4, it can be deduced the values of variables 'A' and 'n' must be known in order to calculate the distance between the receiver and transmitter.

Variable 'A' is the reference RSSI value, which is measured in 1 meter, while 'n' is the signal propagation. These two parameters will change with different environments. Furthermore, 'A' and 'n' are not fixed values. In some papers, researchers use the previous experience and literature to set 'A' and 'n' [33]. This method may be simple, but it lacks accuracy. In this project, the real-time measurement is used to set the values of 'A' and 'n'. The main objective is to define three pairs of checking points and update these parameters in real time.

Step 3 is the most indispensable part of this algorithm; the researchers set three pairs of checking points in the tunnel, with the distances between each pair of checking points already measured. The checking points are depicted in Figure 2.2 and Figure 2.3, where TX1 is checking point 1, TX 2 is checking point 2 and TX 3 is checking point 3.

The distance between the first pair of checking points is 1 meter, which can be used to measure parameter 'A'. The distance between the second pair of checking points is 2 meters

Figure 2.4 Transmitter model

in the project. With the help of 'A' and RSSI in the second checking point, the signal propagation can be calculated by Equation 2.4.

From the previous experiment, it can be observed that the human body also alters the results of the RSSI measurement. Therefore, the purpose of the last checking point is to remove the HBE. The last checking point is set 1.5 meters away from the receiver. When the miner passes through the point in Figure 2.3, the receiver will get the RSSI from the wearable device, which is considered the measured value. Equation 2.4 can be used to calculate the ideal RSSI for 1.5 meters and determine the difference between ideal value and measured value. The difference is denoted as the HBE. After establishing the HBE, the Equation 2.4 can be adjusted as follows:

$$\text{RSSI(dBm)} - \text{HBE} = \text{A} - 10\text{nlg(d)}; \tag{2.12}$$

All three parameters will be transmitted to the computer in real time, and the computer software will correspondingly update Equation 2.12 and calculate the distance.

2.3 Evaluation Algorithm

In order to test the algorithm, the CC2531 from TI Company is used to conduct the experiment. Figure 2.4 shows the transmitter and Figure 2.5 shows the receiver of the testing device. The frequency is set to be 2425 MHz, while the output power is set to be 4dBm.

The testing device is installed in the tunnel of the engineering building of University of

Figure 2.5 Receiver model

Saskatchewan, which is illustrated in Figure 2.6.

For the first checking point, the 'A' is measured to be -30dBm. In the second checking point, the RSSI is measured to be -39dBm. Using the measured 'A' and RSSI at the second checking point,

$$A = -30\text{dBm};$$

$$d = 2m;$$

$$RSSI = -39\text{dBm};$$

the signal propagation 'n' can be calculated as follows:

$$RSSI(\text{dBm}) = \text{A} - 10\text{nlg(d)}; \tag{2.13}$$

It can be derived that $n = 2.9897$. Subsequently, the ideal RSSI in 1.5 meters can be computed with:

$$RSSI(\text{dBm}) = \text{A} - 10\text{nlg}(1.5); \tag{2.14}$$

The measured RSSI is found in the next checking point:

$$RSSI = -35.261\text{dBm};$$

The measured RSSI in the final checking point is -31 dBm. It is fairly straightforward to determine that the difference between the ideal and measured $RSSI$ is 4.261 dBm. Furthermore, the final computation method can be written as:

$$RSSI(\text{dBm}) - \text{HBE} = \text{A} - 10\text{nlg(d)};$$

Figure 2.6 Testing place

$$RSSI(\text{dBm}) - 4.261 = -30 - 10 \times 2.9897 \times \lg(\text{d});$$

$$RSSI(\text{dBm}) = -25.739 - 29.897 \times \lg(\text{d}). \tag{2.15}$$

After building the computation algorithm, some experiments are done and the results are recorded in Table 2.3, with the plot displayed in Figure 2.7.

In Figure 2.7, the x-axis represents the number of measured points and the y-axis represents the distance in meters. There are four lines in Figure 2.7: The solid line in red represents the real distance in the experiment. The dotted line in black represents the computed distances using the Shadowing model. The dash-dotted line in blue represents the computed distances with Gaussian distribution applied to the Shadowing model. The dashed line in green represents the results of the proposed algorithm. It can be easily deduced that the results using the proposed algorithm are optimal in comparison to the Shadowing model. At the first few measuring points, the results of the proposed model are almost identical to the real one. In comparing the results of the Shadowing model with the model applied with Gaussian distribution, it can be discerned that the Shadowing model with Gaussian distribution demonstrates enhanced performance. Therefore, applying Gaussian distribution can reduce the measuring errors and result in superior performance.

The average difference between the actual distance and measured distance can be calcu-

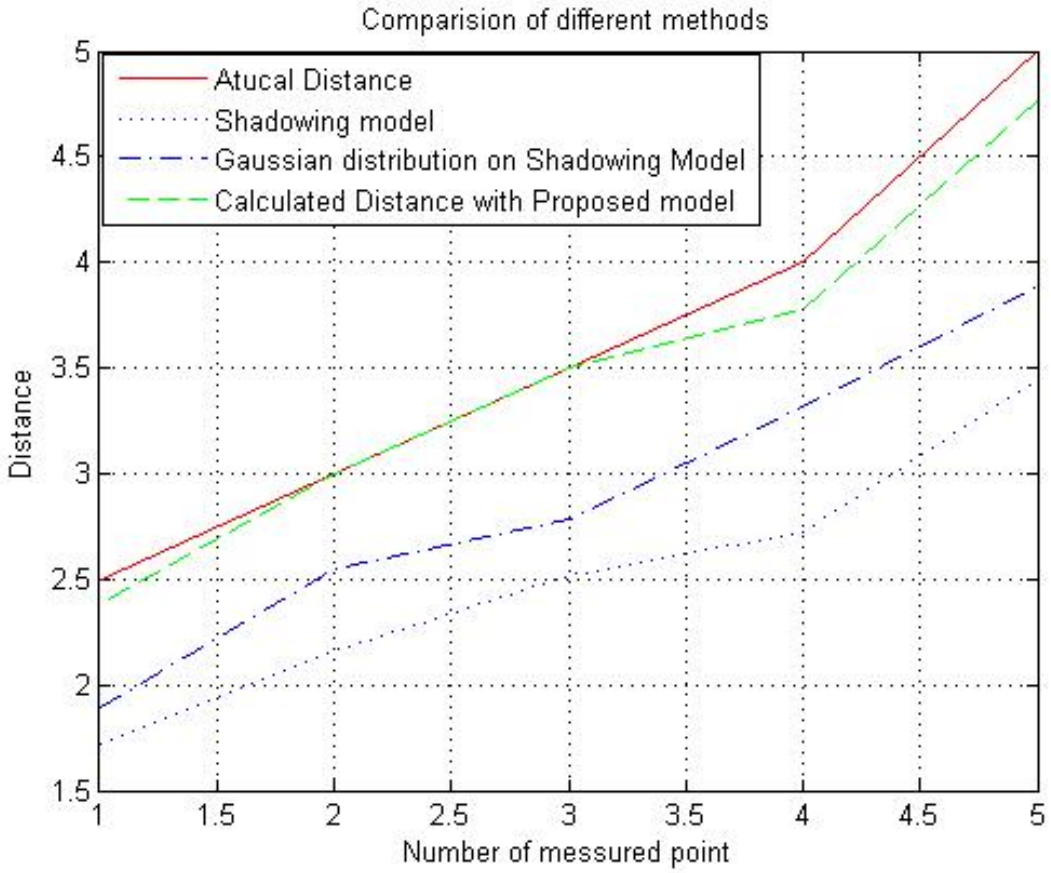

Figure 2.7 Comparison of real distance, measured distance and the distance after algorithm

Table 2.3 Final Results

Actual distance (m)	Calculated distance with Shadowing model (m)	Calculated distance with Gaussian distribution on Shadowing model [34] (m)	Calculated distance with Proposed model (m)
2.5	1.7145	1.8921	2.381
3	2.1601	2.5453	3.0001
3.5	2.5199	2.7822	3.4999
4	2.7216	3.3212	3.7799
5	3.4516	3.8903	4.79669

lated as:

$$\begin{aligned}&((2.5-2.381)+(3.0001-3)+(3.5-3.4999)+\\&(4-3.7799)+(5-4.7669))/5=0.1145.\end{aligned} \tag{2.16}$$

It can be discerned that the difference becomes greater as the distance is increased; the main rationale is that the change of RSSI becomes smaller when the distance is larger. Therefore, it is advantageous to measure the distance using an RSSI within a short distance.

2.3.1 Future work

Although the results from the proposed model are optimal to those of the existed models, some improvements that can still be made in order to further enhance performance.

- The experiments are conducted in the university building, where many types of signals exist at the same frequency. This interference will undoubtedly affect the results. To test the working performance of the system in a more optimal manner, the next experiment ought to be conducted in an underground mine.

- In the model, the miner must initially go through certain checking points, which is not convenient for the users. In our future work, we can strive to formulate an automatic method by which to measure the parameters without setting the checking point.

- There are many corners in the mining tunnel. As it stands currently, the model cannot adapt to corners. Furthermore, other solutions ought to be created for the corner predicament.

- The measurement based on RSSI proves to be worse over long distances. In the future, researchers ought to determine the threshold gap between two receivers in order to ensure that the distance is in proper range.

- Using this algorithm consumes extra resources and time. In order to improve system efficiency, the model must correspondingly be improved.

3. Data Transmission

The purpose of localization is to inform the master control room on the ground of each miner's position in real time. Therefore, it is pertinent to find the fastest and most efficient manner by which to transmit the data of each miner to the central computer system.

3.1 Communication Protocol: ZigBee

There are two main methods by which to transmit the data to the master control room: wireless and wired. Both of these have their own respective advantages and disadvantages.

In the mining industry, many miners and visitors may be working in the same area at the same time. The maximum number of connection nodes is imperative to the success of the project. Table 3.1 includes different wireless communication protocols. Upon comparison, ZigBee [35] is selected to be used for the communication protocol, transmitting the data to the master control room on the ground.

The ZigBee protocol was envisaged in 1998 and created in 2003. The protocol was subsequently corrected in 2006. From Table 3.1, it can be observed that the ZigBee can hold as many as 65000 nodes at the same time. Therefore, it meets the requirement of allowing many people to share the communication system simultaneously. In comparison to the wireless communication, wire line communication requires a cable line. However, cable line installation in the underground mine is a difficult endeavour. Therefore, wireless communication is advantageous.

In order to ensure that the device lasts as long as possible, a protocol must be employed that consumes the least amount of power throughout transmission. From Table 3.1, it can be discerned that ZigBee merely consumes an average of 1mW of energy for transmission, with an average peak current consumption of 15.7mA. ZigBee requires less power than both Bluetooth and Wi-Fi. The BLE requires less power than ZigBee; however, its transmission

Table 3.1 Comparisons between different wireless communication protocols

	Data rate (bps)	**Range (m)**	**Power supply (mW)**	**Max node**	**Security**
ZigBee [17]	250k	10-300	1	65,000	128-AES
Bluetooth [36]	3M	10	50-100	8	64/128-bits
BLE [37]	1M	10	0.01-0.5	8	128-AES
Wi-Fi [38]	<11M	10-100	3-6	32	128-AES
Bodycom [39]	<10k	Body to body	3.6×10^{-2}	2	128-AES
NFC [40]	<0.2M	<0.15	less	Point to point	No
Dual-frequency, Passive RFID [41]	128k	2-10	No battery needed	64-1K	No

range is much less than that of ZigBee and it can only connect to 8 nodes simultaneously. The distance for transmission of ZigBee is normally from 10 to 100 meters. Furthermore, ZigBee is the best choice with respect to power consumption.

The disadvantage of the ZigBee is that the data rate is only 250k bits per second, signifying that it takes more time to transmit the same amount of data as compared to most other protocols. However, the application of this system does not require a high-speed transmission method. Moreover, high-speed transmission consumes more power, which is a drawback in the system.

In summary, the ZigBee is the most optical wireless protocol for data transmission.

In this project, 2.4 GHz is chosen to be the working frequency of ZigBee. There are three types of networks supported by ZigBee: star, tree and generic mesh networking. The coordinator device is necessary to build a network. Subsequently, there should be at least one collector to communicate with the coordinator. Sometimes, routers will be able to extend the transmission distance [17].

3.2 Transmission Method

Due to the long distance of the underground tunnel, a facile transmission method is required to transmit the data from the miner to the master control room.

The main objective of the transmission method is to transmit the data packet using transfer nodes. The data collected by any wearable device will be sent to the nearest transfer node first. Then, the transfer node will pass the data package to another transfer node in the direction of the master control room. Finally, the last transfer node will upload the data package to the central computer in the master control room. The data collected by any transfer node also transmits in this transfer node based transmission net. All data collected by the wearable devices and the transfer nodes will finally be transmitted to the central computer and processed. Figure 3.1 illustrates the central idea of this transmission method.

In order to envision the idea, two algorithms were designed for the wearable device and the transfer nodes on the wall.

The wearable device cannot receive data. It can only transmit the data package to the nearest transfer node. The algorithm of the wearable device is depicted in Figure 3.2.

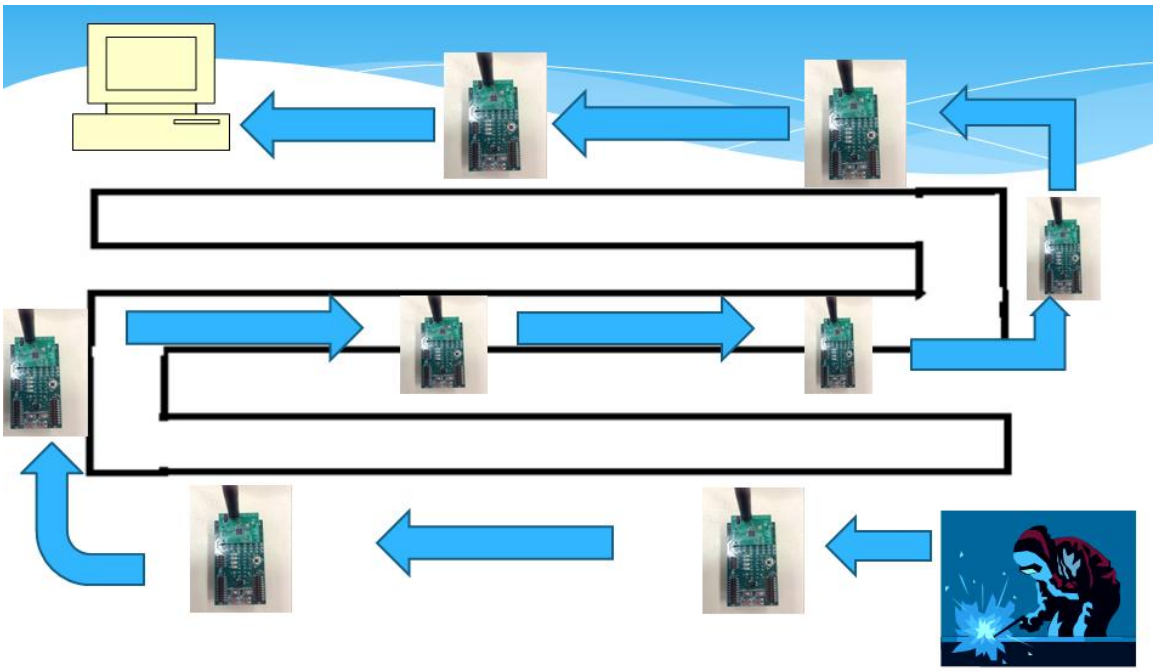

Figure 3.1 Transmission net underground

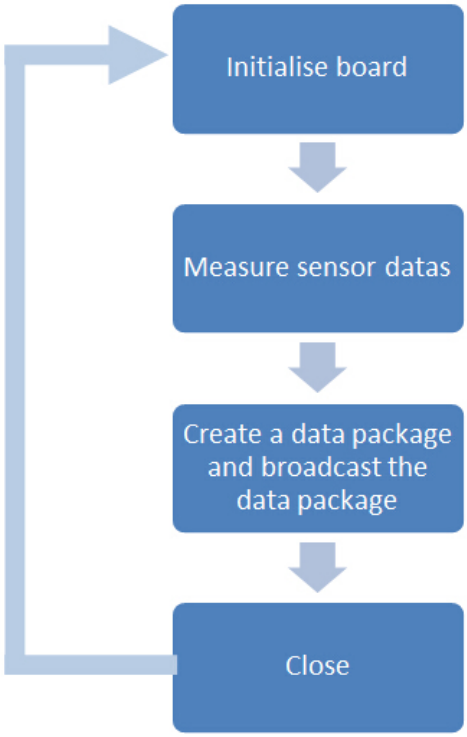

Figure 3.2 The algorithm of the wearable device

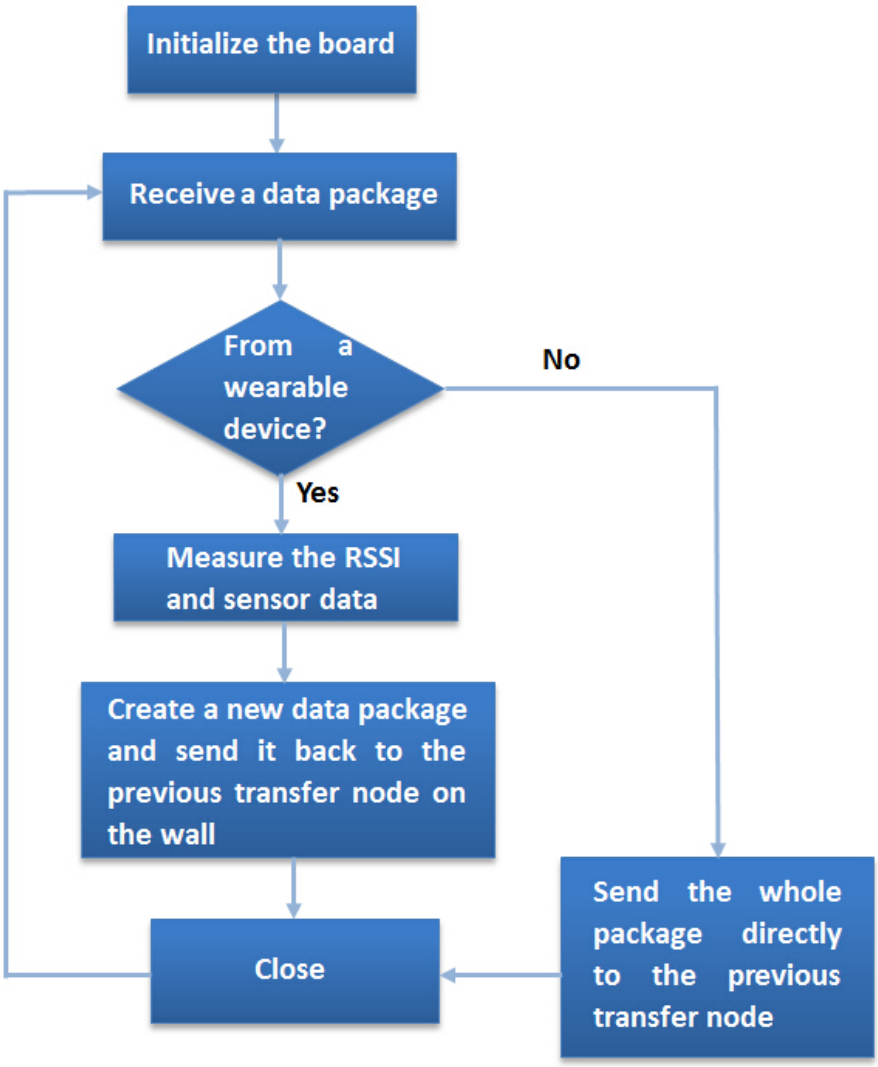

Figure 3.3 The algorithm of the transfer node

The algorithm of the transfer node is depicted in Figure 3.3. When the transfer node operates as a transmitter, its destination is only the previous transfer node, which refers to the neighbour transfer node in the direction of the master control room. This ensures that only effective transmissions are conducted. All of the other transfer nodes will not receive the data package.

In this transmission method, the transfer nodes keep receiving the data from the nearest wearable device and other transfer nodes. When the data is received from a wearable device, the transfer node will measure the RSSI first. It then creates a new data package, which includes the data received from the wearable device tagged with its own RSSI, as well as

the data of the surrounding environment collected by the transfer node itself. The new data package will be transmitted to the previous transfer node. If the transfer node receives the data from its next transfer node, it will only transfer the data to the previous transfer node.

In order to recognize all transmitters and receivers, a unique ID is given to every device. The ID will be tagged to the data package when it is sent out. The central computer can easily recognize which device the data comes from based on the unique ID. With the data transmitting from transfer nodes, the computer can update the location of the miner in real time. The supervisor on the ground can obtain the location directly from the computer.

4. Position Detection Using RSSI

In Chapter 2, a proposed model was developed to measure the distance using RSSI. In this chapter, the RSSI proposed model is utilized to detect the positions of the miners.

4.1 3-point Localization

Consider a miner walking in the mining tunnel as a point moving in a path (depicted in Figure 4.1.). In order to detect the position of the miner in 2D space, a 3-point localization method is applied; this method measures the distance between the miner and three different reference points, and subsequently draws circles to localize the object's position. With this method, at least three circles must be drawn for successful localization.

Figure 4.2 illustrates the 3-point localization method. In Figure 4.2, A, B and C are three reference points and O is the objective point. The positions of these three reference points are known. If the distances between A and O, B and O, and C and O are known as AO, BO and CO, three circles can be drawn with A, B and C as the centers of the circles and AO, BO and CO as the radius' of the circles. O represents the common point of these three circles.

Therefore, in order to localize the position of point O, the distances between A and O, B

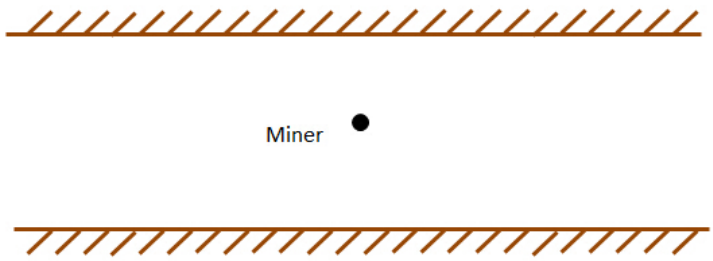

Figure 4.1 2D diagram of a miner walking in the mining tunnel

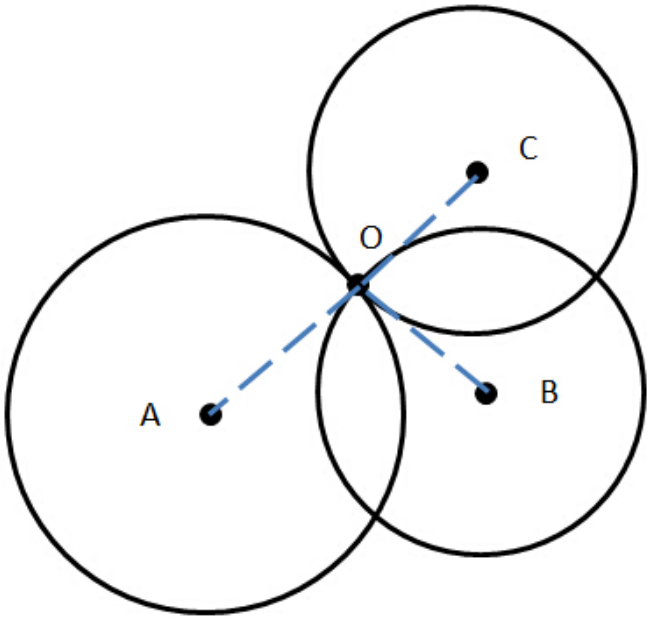

Figure 4.2 3-point localization method [1]

and O, and C and O must be measured. With the help of the reference points, the location of the miner can be determined.

4.2 2-point Localization Method

Figure 4.3 illustrates a 3-point localization method, but with only two circles drawn. A and B represent the two reference points, as well as the centers of the circles. P1 and P2 are the two common points of these two circles.

It can be deduced from Figure 4.3 that, if only two circles are drawn with the 3-point

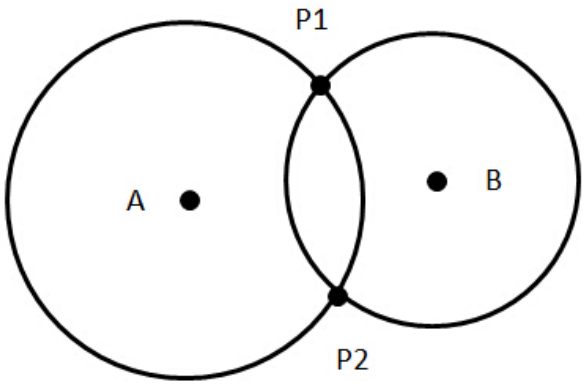

Figure 4.3 Localization with 2 reference points

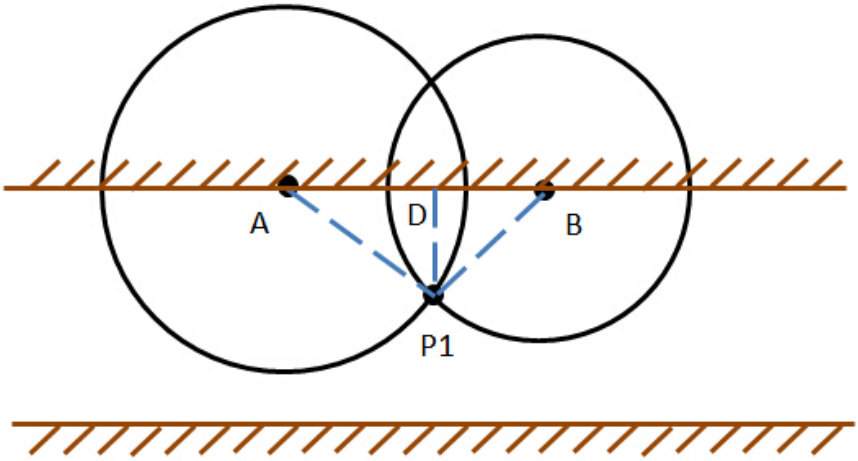

Figure 4.4 Diagram showing the computation using 2-point localization method

localization method, there will be only two common points (P1 and P2), either of which could represent the miner. This signifies that there are some difficulties in finding the final location of the miner. However, in this project, the miner walks in the mining tunnel, as Figure 4.4 represents. It can be observed that, with two reference points A and B, there are two common points P1 and P2. In this situation, it is apparent that only one common point, P1, is located in the tunnel and the other one, P2, is located inside the wall. Therefore, the common point P2 can be ruled out. The only possible point of the miner should be P1.

This method only uses two reference points and is referred to as the "2-point Localization Method". This method requires that only two distances must be measured: AP1 and BP1. With the help of reference points A and B, the position of the miner can be determined. The flow chart of the 2-point localization method is depicted in Figure 4.5.

4.2.1 Computation Process

Using the 2-point localization method, two triangles can be drawn to calculate the position of the miner. As Figure 4.4 reveals, a line vertical to the wall is drawn and the common point is set to be D. Subsequently, two triangles appear: triangle ADP1 and triangle BDP1.

From Figure 4.6, it can be observed that there are two triangles in the two circles. Let

$$AP1 = a;$$

$$BP1 = b;$$

$$AB = c;$$

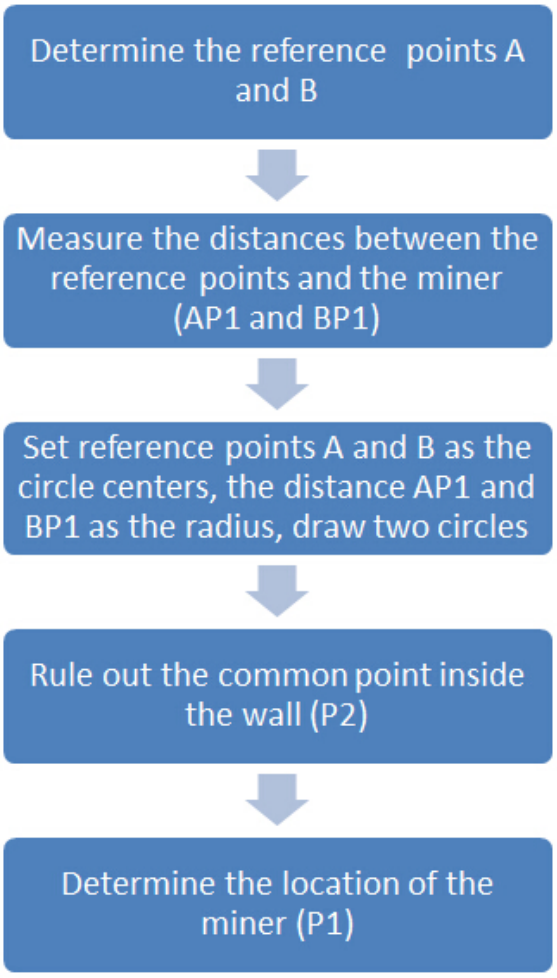

Figure 4.5 Working principle of the 2-point localization method

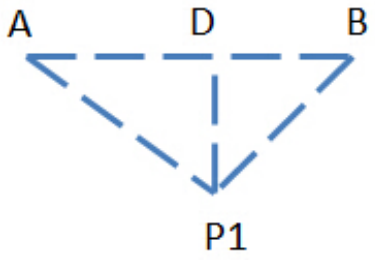

Figure 4.6 Triangles diagram for the computation using 2-point localization method

In order to localize the position of point P1, the distance between reference point A and point D and the distance between point P1 and point D should be computed. Set

$$AD = x;$$

$$DP1 = y;$$

Apply the Pythagorean theorem to triangle ADP1,

$$DP1 = AP1^2 - AD^2;$$

which gives:

$$y^2 = a^2 - x^2; \tag{4.1}$$

Apply the Pythagorean theorem to triangle BDP1,

$$DP1 = BP1^2 - BD^2;$$

which gives:

$$y^2 = b^2 - (c - x)^2; \tag{4.2}$$

Equation 4.1 and 4.2 give:

$$a^2 - x^2 = b^2 - (c - x)^2; \tag{4.3}$$

$$x = \frac{a^2 - b^2 + c^2}{2c}; \tag{4.4}$$

Combining Equation 4.4 and Equation 4.1 gives:

$$y = \sqrt{a^2 - \frac{(a^2 - b^2 + c^2)^2}{4c^2}}. \tag{4.5}$$

With Equation 4.4 and 4.5, the length of AD and DP1 can be computed.

In order to localize the position of point P1, it is critical that a Cartesian coordinate system is built. As Figure 4.7 illustrates, Point A is set as the original point $(0, 0)$ and line AB is set to be the x-axis. The line goes through point A vertically, with AB set to be the y-axis. Subsequently, the coordinate of point B is $(c, 0)$ and that of point D is $(\frac{a^2-b^2+c^2}{2c}, 0)$. Furthermore, point P1's coordinate, which represents the miner's position, is $(\frac{a^2-b^2+c^2}{2c}, \sqrt{a^2 - \frac{(a^2-b^2+c^2)^2}{4c^2}})$, as compared to reference point A.

The computation and working principle of the 2-point reference method is summarized as a flow chart in Figure 4.8.

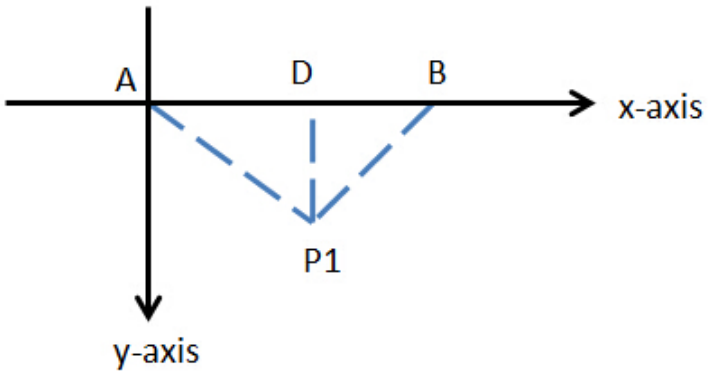

Figure 4.7 Localization using Cartesian coordinate system

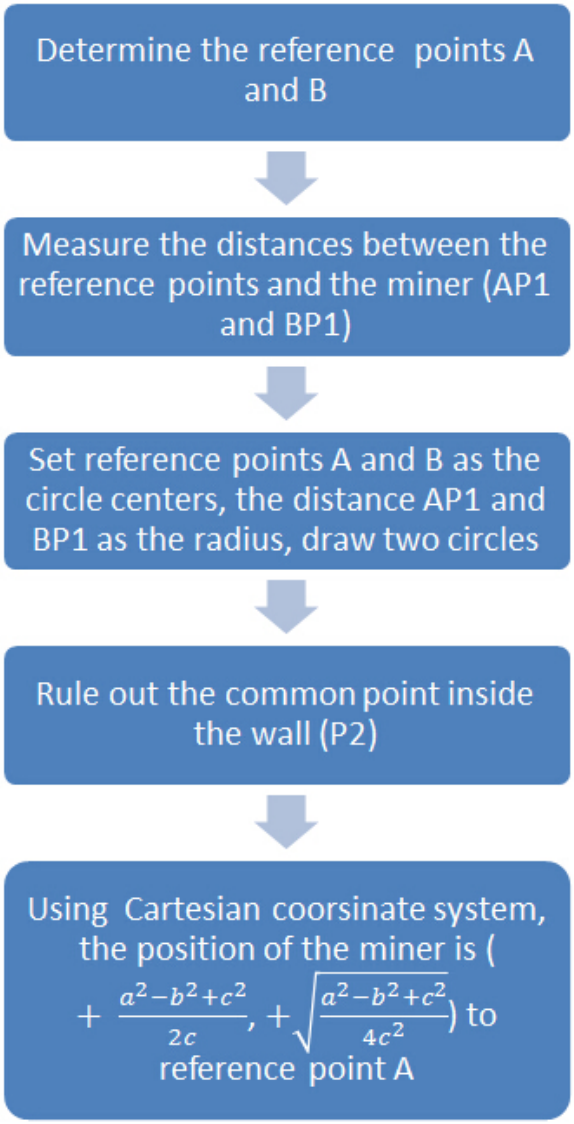

Figure 4.8 Computation and working principle of the 2-point localization method

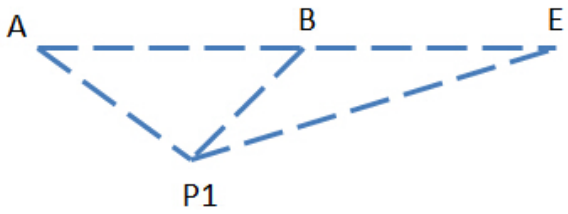

Figure 4.9 The diagram showing the improved 2-point localization method

4.3 Improved 2-point Localization Method

The 2-point localization method works, but lacks accuracy. For example, when the reference point measures the distance to the miner, the measurement may not be very accurate; this, in turn, impedes the accuracy of determining the miner's real position. To minimize the error, an advanced version of the 2-point localization method is developed.

In the mining tunnel, many transfer nodes (reference points) are installed on the wall every 4 meters. When a miner is walking in the mining tunnel, the transmitter on the miner will automatically connect to the receiver within its coverage. For the 2-point localization method, only the nearest two receivers are used for localization. To improve the accuracy of localization, the nearest three receivers can be used to compute the position of the miner.

As Figure 4.9 depicts, points A, B and E are the three nearest reference points to the miner P1. With points A and B, the 2-point localization computation method introduced in the last section can be used to compute the miner's position (denoted '$P1_{AB}$'). Subsequently, with points A and E, the miner's position can be computed (denoted '$P1_{AE}$'), as well as with point B and E (denoted '$P1_{BE}$'). If there is no error, these three positions should be the same; however, this is rarely the case. Normally, the three positions are different and the average of the three computed positions is used to represent the position of the miner. In this manner, the accuracy of the localization is theoretically better.

This method is named "the improved 2-point localization method". Its computation procedure is provided in the next subsection.

4.3.1 The Improved Computation Process

In the improved 2-point localization method, three reference points with the miner forms three triangles. To make the computation process more mainstream, a Cartesian coordinate system is built, as depicted in Figure 4.10. In Figure 4.10 , the reference points A, B and

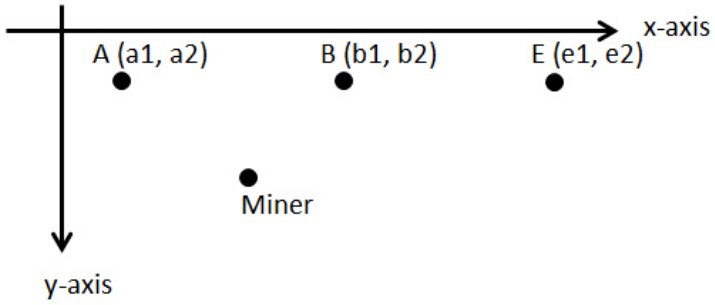

Figure 4.10 Diagram shows the Cartesian coordinate system with improved 2-point localization method

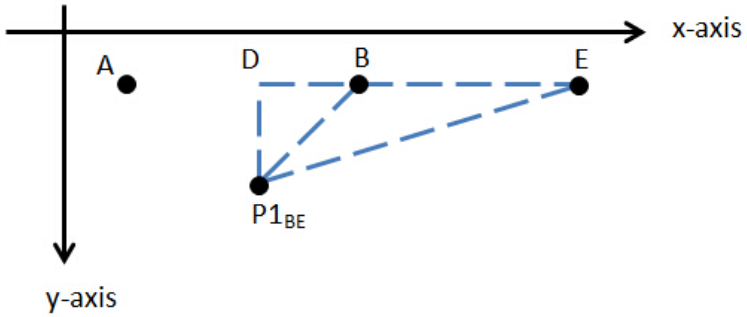

Figure 4.11 An example diagram showing the computation using the improved 2-point localization method

E do not have unique positions in the Cartesian coordination system. One can assume that the coordinates of these three points are $(a1, a2), (b1, b2)$ and $(e1, e2)$.

Reference points B and E can be used as an example to compute the position of the miner. Assume the measured distance from reference point B to the miner is $BP1_{BE}$, and from reference point E to the miner is $EP1_{BE}$. Consider point B as the centre and $BP1_{BE}$ as the radius in order to draw a circle, and consider point E as the centre and $EP1_{BE}$ as the radius in order to draw the other one. The cross point located in the tunnel signifies the position of the miner, which is denoted $P1_{BE}$.

As Figure 4.11 illustrates, a line vertical to the mining wall (ABE) is drawn and the common point is set to be D. Subsequently, two triangles appear: triangle $BDP1_{BE}$ and triangle $DEP1_{BE}$. Let

$$BP1_{BE} = a;$$

$$EP1_{BE} = b;$$

$$BE = c;$$

From Section 4.2.1, it can be inferred that, in comparison to reference point B, point $P1_{BE}$'s coordinate (which is also the miner's position) is

$$(\frac{a^2 - b^2 + c^2}{2c}, \sqrt{a^2 - \frac{(a^2 - b^2 + c^2)^2}{4c^2}}), \tag{4.6}$$

which can also be written as

$$(\frac{BP1_{BE}^2 - EP1_{BE}^2 + BE^2}{2BE}, \sqrt{BP1_{BE}^2 - \frac{(BP1_{BE}^2 - EP1_{BE}^2 + BE^2)^2}{4BE^2}}); \tag{4.7}$$

Considering the fact that point B has coordinate $(b1, b2)$, the coordinate of point $P1_{BE}$ as measured by the triangle is

$$\begin{aligned} P1_{BE}(b1 + \frac{BP1_{BE}^2 - EP1_{BE}^2 + BE^2}{2BE}, \\ b2 + \sqrt{BP1_{BE}^2 - \frac{(BP1_{BE}^2 - EP1_{BE}^2 + BE^2)^2}{4BE^2}}); \end{aligned} \tag{4.8}$$

For reference points A and B, the cross point of circles A and B located in the tunnel is denoted $P1_{AB}$. Using the 2-point localization method for triangle $ABP1_{AB}$, the coordinate of the miner (point $P1_{AB}$) can be computed. The result should be:

$$\begin{aligned} P1_{AB}(a1 + \frac{AP1_{AB}^2 - BP1_{AB}^2 + AB^2}{2AB}, \\ a2 + \sqrt{AP1_{AB}^2 - \frac{(AP1_{AB}^2 - BP1_{AB}^2 + AB^2)^2}{4AB^2}}); \end{aligned} \tag{4.9}$$

For reference points A and E, the cross point of circles A and E located in the tunnel is denoted $P1_{AE}$. Using the 2-point localization method for triangle $AEP1_{AE}$, the coordinate of the miner (point $P1_{AE}$) can be computed. The result should be:

$$\begin{aligned} P1_{AE}(a1 + \frac{AP1_{AE}^2 - EP1_{AE}^2 + AE^2}{2AE}, \\ a2 + \sqrt{AP1_{AE}^2 - \frac{(AP1_{AE}^2 - EP1_{AE}^2 + AE^2)^2}{4AE^2}}); \end{aligned} \tag{4.10}$$

The known, measured and computed parameters are listed in Table 4.1. Finally, we are able to determine the average of these three positions with respect to the accurate position of the miner (P1).

$$P1 = \frac{P1_{AB} + P1_{AE} + P1_{BE}}{3}. \tag{4.11}$$

Table 4.1 The parameters for the computation of the improved 2-point localization method

	Known position	**Measured distance (m)**	**Computed position**
Triangle $ABP1_{AB}$	Point A, B	$AP1_{AB}$, $BP1_{AB}$	$P1_{AB}$
Triangle $AEP1_{AE}$	Point A, E	$AP1_{AE}$, $EP1_{AE}$	$P1_{AE}$
Triangle $BEP1_{BE}$	Point B, E	$BP1_{BE}$, $EP1_{BE}$	$P1_{BE}$

$P1_{AB}$,$P1_{AE}$ and $P1_{BE}$ are all vectors in table 3.1. The computation and working principle of the improved 2-point reference method is summarized in a flow chart, as depicted in Figure 4.12.

4.4 Test and Comparison

The 2-point localization method and the improved method are discussed in Section 4.2 and 4.3. In this section, the localization results of these two methods will be introduced and compared to the real positions. The test environment and method will be introduced first, followed by the test results.

The test is conducted in the College of Engineering tunnel at the University of Saskatchewan. The schematic of the system installation in the tunnel is illustrated in Figure 4.13. Points A, B and C represent three transfer nodes, which are also the reference points mentioned in the computation methods. They are installed in a line on the wall, with the height set to be 1 meter. The miner, who is also the tester, will wear the wearable device and walk past the three transfer nodes, one by one from left to right. All three positions of reference points are measured by the tap measure. The tester is asked to stand on every specific point in order to measure the RSSI. All data is recorded and processed using the algorithm.

Figure 4.14 demonstrates the scale of the testing place. The two solid vertical lines in red at the furthest left and the furthest right represent the starting and finishing line for the tester. The tester will walk at a constant velocity from the starting line to the finishing line. The starting line is located 2 meters before the first transfer node A and the finishing line is located 2 meters after the last transfer node C. The three transfer nodes are placed uniformly on the wall, with the separation distance set to be 4 meters.

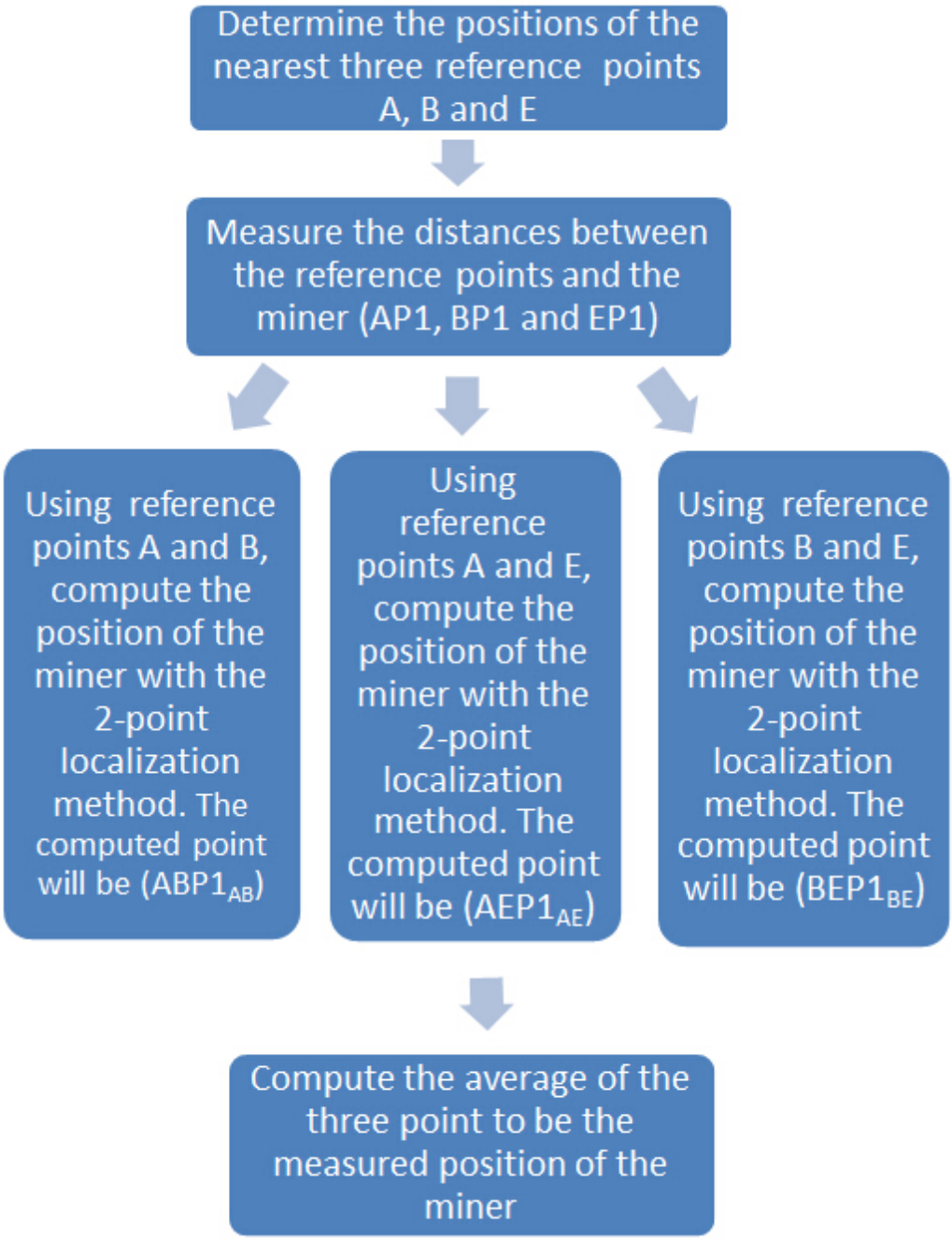

Figure 4.12 Computation and working principle of the improved 2-point localization method

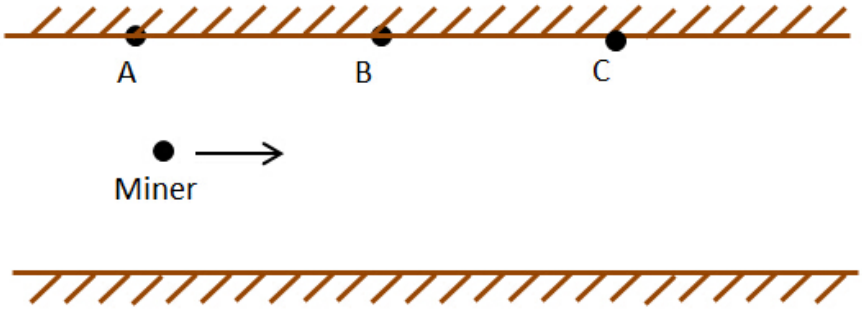

Figure 4.13 The 2-D schematic of the testing place

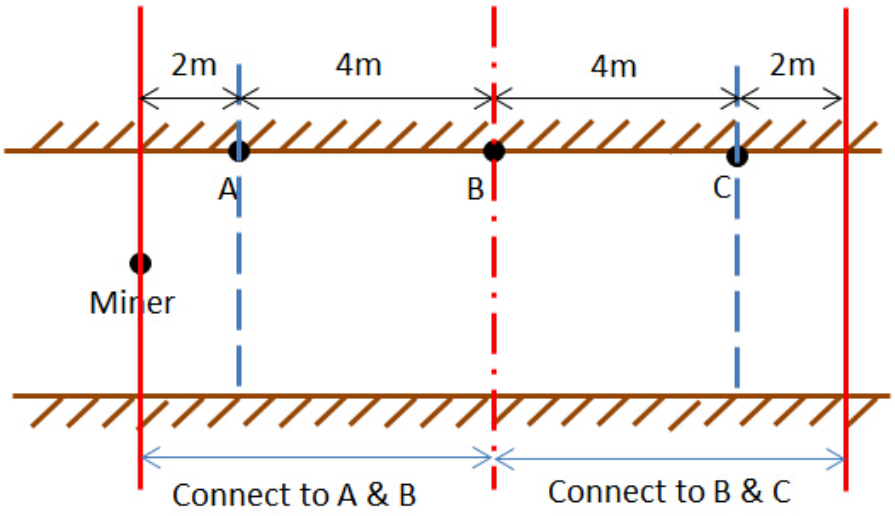

Figure 4.14 The schematic of the testing place with scale

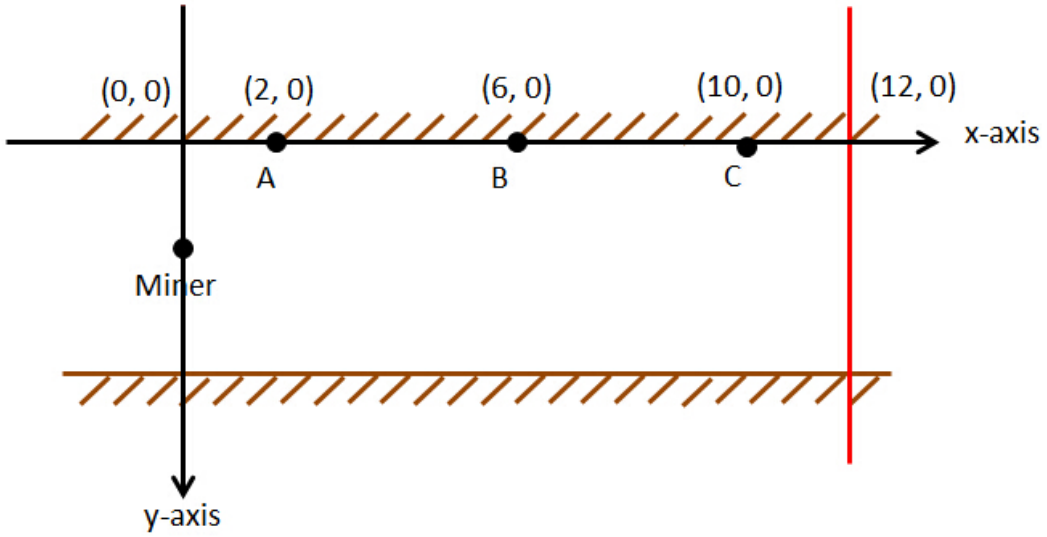

Figure 4.15 The Cartesian coordinate system for testing

For the 2-point localization method, when the tester is moving, the nearest two transfer nodes will be connected and their data will be used for position computation. As Figure 4.14 illustrates, the dash-dot vertical line crossing point B represents the boundary of the working area of transfer nodes A and C. When the tester is walking in the left half, the data measured by transfer nodes A and B will be used for localization. Contrastingly, when the tester is located in the right half in relation to the boundary, the data measured by transfer nodes B and C will be collected.

For the improved 2-point localization method, the data measured by all three transfer nodes will be collected for position computation.

In order to localize the tester, a Cartesian coordinate system is built as Figure 4.15 depicts. The cross point of the starting line and the wall is set to be the original point. The x-axis is along the wall to the right and the y-axis is the along the starting line in a downward direction. Additionally, the coordinate of point A is $(2, 0)$, that of point B is $(6, 0)$ and that of point C is $(10, 0)$.

The tests are conducted several times and three cases are revealed in the following subsections.

Table 4.2 The real positions of the tester and positions measured by the 2-point localization method and the improved method for the first test [1]

Real Positions (m)	Positions measured by the 2-point localization method (m)	Positions measured by the improved 2-point localization method (m)
(0, 1)	(0.83, 0.92)	(-0.73, 1.15)
(2, 1)	(1.57, 1.06)	(1.76, 0.64)
(4, 1)	(4.51, 1.56)	(3.49, 1.23)
(6, 1)	(6.51, 1.87)	(6.44, 1.29)
(8, 1)	(7.76, 0.26)	(7.72, 1.37)
(10, 1)	(10.14, 1.14)	(10.04, 0.93)
(12, 1)	(11.15, 0.94)	(11.50, 0.84)

4.4.1 The First Test: Tester walks close to the transfer nodes

In the first test, the tester wearing the wearable device walks in a straight line and is located 1 meter away from the transfer nodes.

The real positions, the positions measured by the 2-point localization method and the positions measured by the improved 2-point localization method for the first test, are listed in Table 4.2.

The comparisons between the real positions are revealed in Figure 4.16. In Figure 4.16, the solid black line tagged with circles represents the real positions of the tester. It can be observed that the tester walks in a straight line, which is located 1 meter away from the x-axis. The dashed blue line tagged with stars represents the positions measured by the 2-point localization method. The dash-dot line in red tagged with diamonds represents the positions measured by the improved 2-point localization method.

From Figure 4.16, it can be deduced that the improved method demonstrates a better performance than the 2-point localization method. One may compute the difference of distance between each pair of real and measured positions. For the 2-point localization method, the average error distance is 0.6939 meters and the maximum error distance is 1.0055 meters. For the improved 2-point localization method, the average error distance

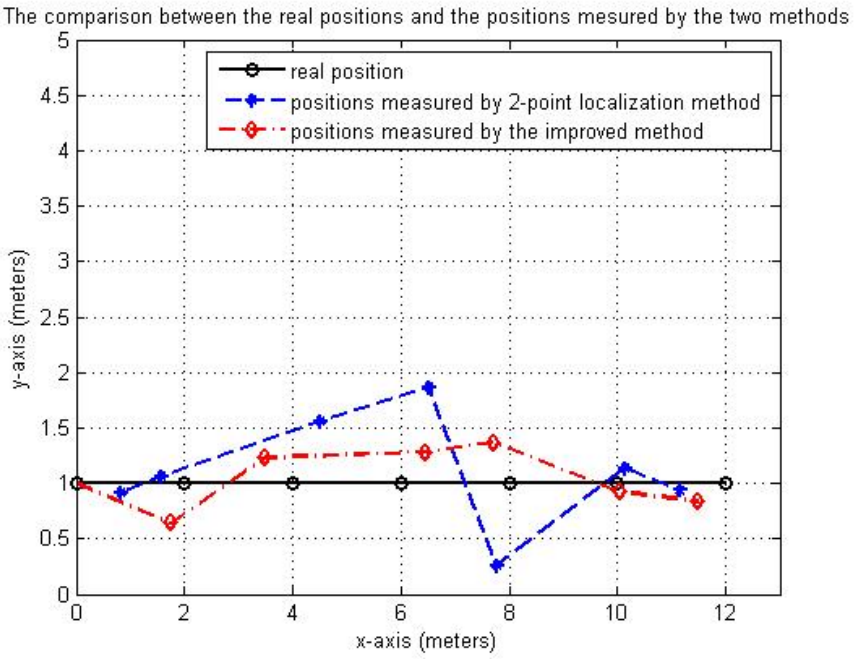

Figure 4.16 Building a Cartesian system for the tester, the figure shows the comparisons among the real positions, the positions measured by the 2-point localization method and the positions measured by the improved method for the first test

Table 4.3 The comparison data of the 2-point localization method and the improved 2-point localization method for the first test

	Positions measured by the 2-point localization method	Positions measured by the improved 2-point localization method
The maximum error distance (m)	1.01	0.75
The average error distance (m)	0.69	0.48
The minimum error distance (m)	0.19	0.09

Table 4.4 The real positions of the tester and positions measured by the 2-point localization method and the improved method for the second test

Real Positions (m)	Positions measured by the 2-point localization method (m)	Positions measured by the improved 2-point localization method (m)
(0, 3)	(-0.52, 3.78)	(-0.60, 2.99)
(2, 3)	(1.22, 3.27)	(1.49, 2.98)
(4, 3)	(3.20, 2.67)	(3.58, 2.74)
(6, 3)	(6.81,3.03)	(5.87, 3.64)
(8, 3)	(8.18, 2.78)	(7.28, 2.79)
(10, 3)	(10.11, 2.07)	(10.64, 3.38)
(12, 3)	(11.22, 2.43)	(12.71, 3.45)

is 0.4774 meters and the maximum error distance is 0.7479 meters. The data included in Table 4.3 reveals that the performance of the improved method is superior.

4.4.2 The Second Test: Tester walks far from the transfer nodes

In the second test, the tester walks in a straight line and is located 3 meters away from the transfer nodes. As compared to the first test, the tester is located further away from the transfer nodes.

The real positions, the positions measured by the 2-point localization method and the positions measured by the improved 2-point localization method for the second test, are listed in Table 4.4.

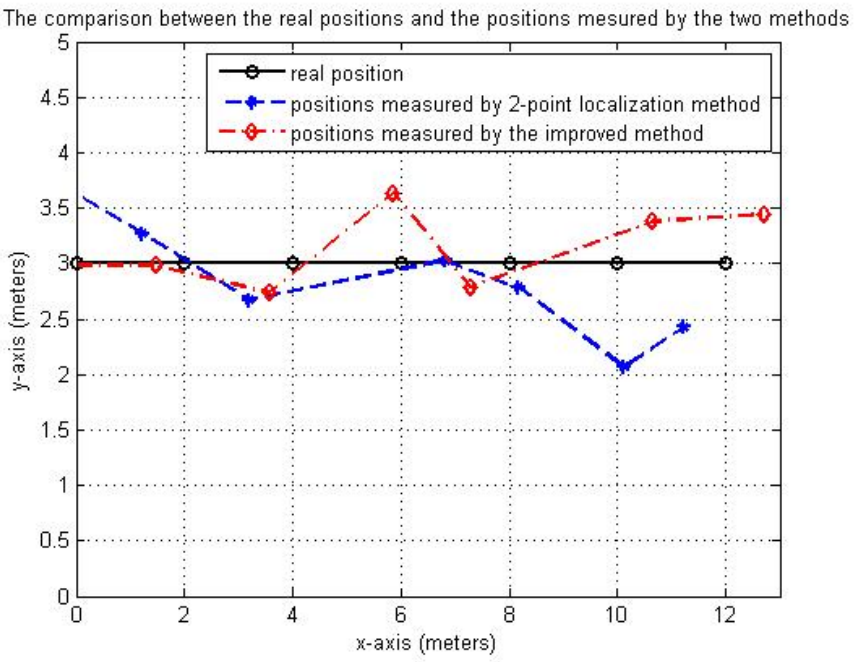

Figure 4.17 Building a Cartesian system for the tester, the figure illustrates the comparisons between the real positions, the positions measured by the 2-point localization method and the positions measured by the improved method for the second test

The comparisons between the real positions are revealed in Figure 4.17. In Figure 4.17, the solid black line tagged with circles represents the real positions of the tester. It can be observed that the tester walks in a straight line, which is located 3 meters away from the x-axis. The dashed blue line tagged with stars represents the positions measured by the 2-point localization method. The dash-dot line in red tagged with diamonds represents the positions measured by the improved 2-point localization method.

From Figure 4.17, it can be deduced that the improved method imparts a better performance than the 2-point localization method, especially with regards to the measurement of the coordinates of the x-axis. One may compute the difference of distance between each pair of real and measured positions. For the 2-point localization method, the average error distance is 0.8033 meters and the maximum error distance is 0.9683 meters. For the improved 2-point localization method, the average error distance is 0.6559 meter and the maximum error distance is 0.8412 meters. Therefore, the average performance of the improved 2-point

Table 4.5 The comparison data of the 2-point localization method and the improved 2-point localization method for the second test

	Positions measured by the 2-point localization method	Positions measured by the improved 2-point localization method
The maximum error distance (m)	0.97	0.84
The average error distance (m)	0.80	0.66
The minimum error distance (m)	0.28	0.49

localization method is superior to that of the 2-point localization method. The data included in Table 4.5 supports these findings.

In comparing the average error distance of the second test with the first test, it can be deduced that when the distance between the miner and the transfer nodes becomes greater, the average performance will decline. This conclusion matches the findings outlined in Chapter 2.

4.4.3 The Third Test: Tester walk in a curve

In the third test, the tester walks in a curve, which begins 3 meters away from the x-axis, then proceeds to walk closer (1 meter away), and then walks as far as 3 meters away. Finally, the tester walks close to the a-axis again at 1 meter.

The real positions, the positions measured by the 2-point localization method and the positions measured by the improved 2-point localization method for the third test, are listed in Table 4.6.

The comparisons between the real positions, the positions measured by the 2-point localization method and the positions measured by the improved 2-point localization method, are revealed in Figure 4.18. In Figure 4.18, the solid black line tagged with circles represents the real positions of the tester. It can be observed that the tester walks in a curve, which constantly moves toward and away from the a-axis. The dashed blue line tagged with stars represents the positions measured by the 2-point localization method. The dash-dot line in red tagged with diamonds represents the positions measured by the improved 2-point localization method.

Table 4.6 The real positions of the tester and positions measured by the 2-point localization method and the improved method for the third test

Real Positions (m)	Positions measured by the 2-point localization method (m)	Positions measured by the improved 2-point localization method (m)
(0, 3)	(-0.24, 2.43)	(0.12, 2.58)
(2, 2)	(2.31, 2.49)	(2.19, 2.42)
(4, 1)	(3.87, 0.89)	(4.41, 1.05)
(6, 2)	(6.51, 2.31)	(6.28, 1.80)
(8, 3)	(6.99, 2.11)	(8.51, 2.77)
(10, 2)	(9.37, 1.90)	(9.57, 2.41)
(12, 1)	(11.61,1.64)	(11.79, 1.61)

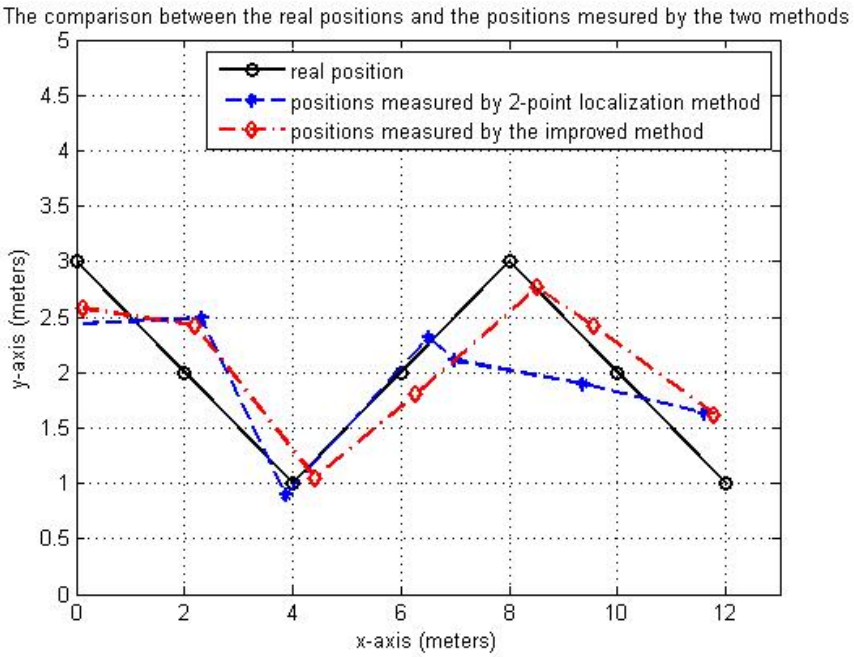

Figure 4.18 Building a Cartesian system for the tester, the figure shows the comparisons between the real positions, the positions measured by the 2-point localization method and the positions measured by the improved method for the third test

Table 4.7 The comparison data of the 2-point localization method and the improved 2-point localization method for the third test

	Positions measured by the 2-point localization method	Positions measured by the improved 2-point localization method
The maximum error distance (m)	1.34	0.65
The average error distance (m)	0.67	0.50
The minimum error distance (m)	0.17	0.34

From Figure 4.18, it can be deduced that the improved method gives a better performance as compared to the 2-point localization method. One may compute the difference of distance between each pair of real and measured positions. For the 2-point localization method, the average error distance is 0.6694 meters and the maximum error distance is 1.3412 meters. For the improved 2-point localization method, the average error distance is 0.4956 meters and the maximum error distance is 0.6492 meters. The data included in Table 4.7 substantiates the fact that the performance of the improved method is superior.

In comparing the performance of the third case to the previous two, it can be deduced that regardless of how the tester walks, the improved 2-point localization method will always offer superior performance.

For this test system, the testing area is $60m^2$ in total and the three transfer nodes are included in this area. The average area per transfer node is $20m^2$. From the measured and computed data, it can be discerned that the accuracy of the 2-point localization method is approximately 1.5 meters. In contrast, the accuracy of the improved 2-point localization method is approximately 0.9 meters, which is far better than that of the 2-point localization method.

As compared to the existing method, the improved 2-point localization method demonstrates optimal performance. As established in Dr. Rainer Mautz's thesis [42], in a $432m^2$ testing area, 8 transfer nodes work together to measure distance using RSSI. The average area per transfer node is $54m^2$. The reported accuracy is 3 meters.

Although the average coverage per node for our test is less ($20m^2$ and $54m^2$), the perfor-

mance of our localization is far better (0.9m and 3m).

5. Sensor Implementation

In spite of distance measurement and localization, another function of the wearable device is its ability to monitor the human body and detect the environment around the miner. In order to achieve this, some sensors are installed on the wearable devices and the transfer nodes on the wall. The sensors are able to detect and collect relevant data, of which they send back to the master control room on the ground.

Sensors are installed on the development board CC2530. The CC2530 development kit is illustrated in Figure 5.1. The CC2530 is created by a company named Texas Instruments. The IEEE 802.15.4 based protocols can be built in this chip. The Zigbee stack can be installed in this development board.

Figure 5.2 depicts the schematic of CC2530. It can be discerned that the CPU (central processing unit) of the CC2530 development board is the enhanced 8051. The chip has 3 memory buses, which are SFR (special function register), DATA (memory data bus) and XDATA (external memory data bus). Additionally, the CPU also has debug interface and another interrupt unit with 18 inputs.

The enhanced 8051 also uses the original instruction set. However, the enhanced version is much faster than the standard 8051, as the useless bus states are forbidden. At the same time, one clock per instruction cycle in the enhanced 8051 is 12 times faster than the standard version. In the enhanced 8051 CPU, there are four different spaces for memory, which are divided based on the program and data memory. The first memory space is for CODE. This is a read-only memory which has 64 KB. The DATA memory space is for both read and write. This memory space is addressed for 256 bytes. The XDATA is also a read-or-write memory space, which requires 4 to 5 CPU instruction cycles. Normally, the CODE and XDATA will use the same bus on the CPU core. Finally, the SFR memory space will contain 128 bytes,

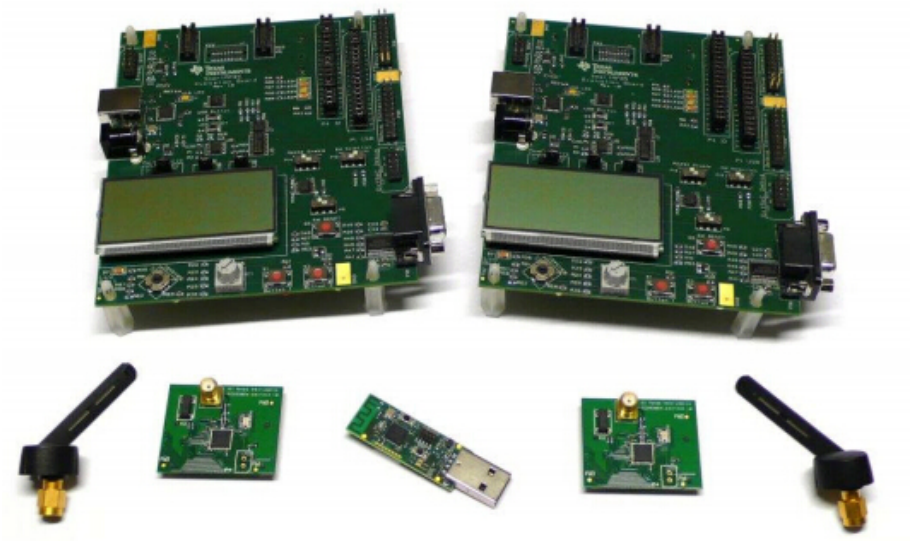

Figure 5.1 CC2530 development kit [7]

of which the address is divided by 8 bits. Every bit can be addressed individually.

5.1 Power Supplement and Peripherals

The CPU and all peripherals must be supplied by the power of 1.8 volts. The CC2530 has three different modes for the low-power application, which are PM1, PM2 and PM3. These three modes can allow the battery to last for a longer amount of time. The advantage of the CC2530 is that it has many different peripherals, which can develop many applications.

In order to connect the micro controller unit (MCU) to sensors, the development board should have some general-propose I/O pins. In the MCU, there are three 8-bits ports which are denoted P0, P1 and P2. Each port has 8 individual pins to connect to the sensor in order to obtain the data. Among these 24 pins, there are two high pins- P1.0 and P1.1, both of which have a 20-mA output. Others merely have a 4mA output current. These general-purpose pins can be used to create interruptions if they are set as inputs. The interruptions can be set to the edge of rising or falling of the external signal. If the general-purpose is not used to generate the interruption, the I/O pins can also be set as different peripheral functions.

From the Figure 5.3, it can be easily discerned that each pin has different peripheral functions. This is the most important tool in order for the user to obtain the data from different sensors. From the table in Figure 5.3, it can be observed that the MCU has

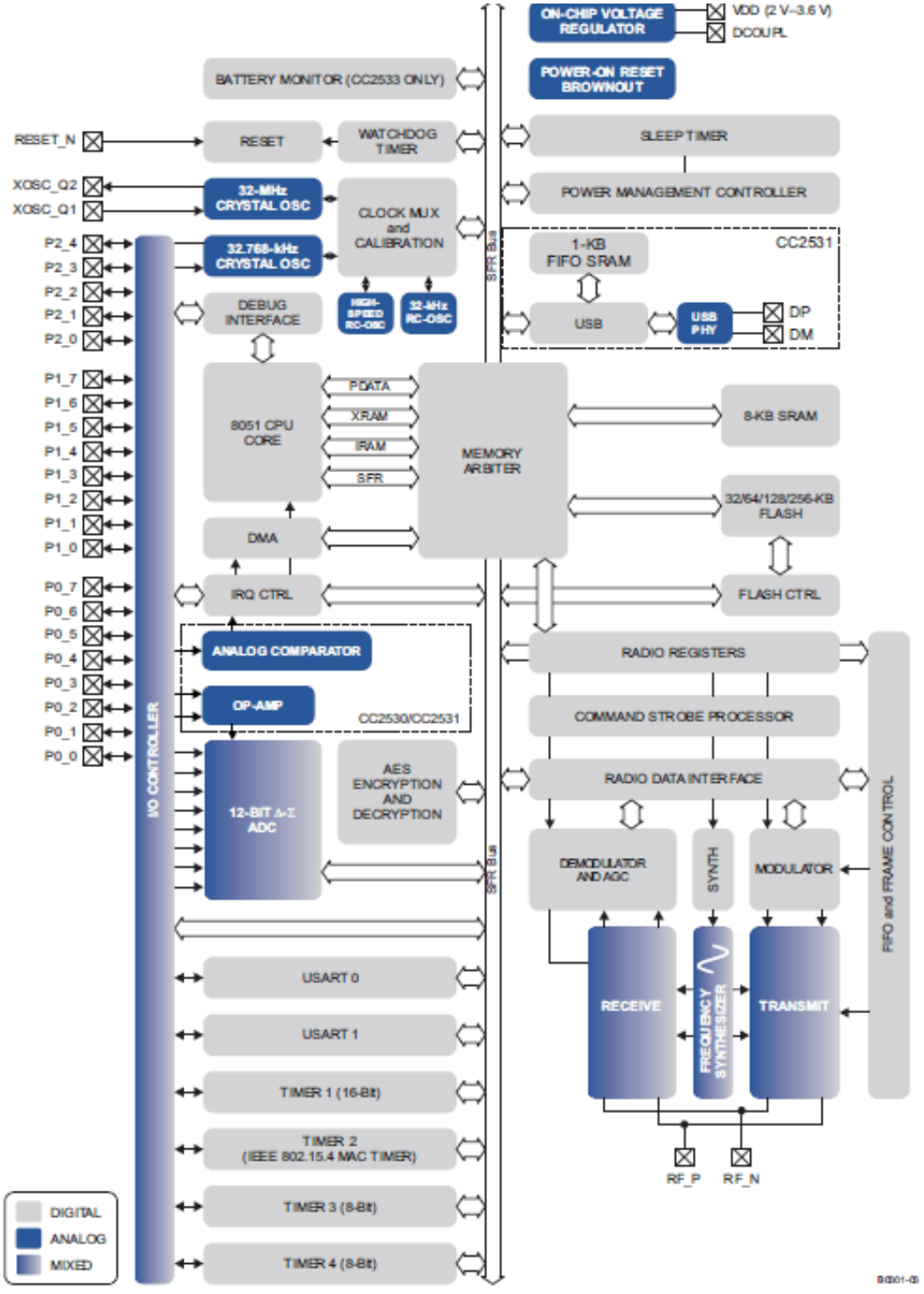

Figure 5.2 CC2530 Schematic [8]

Periphery/ Function	P0								P1								P2				
	7	6	5	4	3	2	1	0	7	6	5	4	3	2	1	0	4	3	2	1	0
ADC	A7	A6	A5	A4	A3	A2	A1	A0													T
Operational amplifier						O	−	+													
Analog comparator			+	−																	
USART 0 SPI			C	SS	MO	MI															
Alt. 2											M0	MI	C	SS							
USART 0 UART			RT	CT	TX	RX															
Alt. 2											TX	RX	RT	CT							
USART 1 SPI			MI	M0	C	SS															
Alt. 2									MI	M0	C	SS									
USART 1 UART			RX	TX	RT	CT															
Alt. 2									RX	TX	RT	CT									
TIMER 1		4	3	2	1	0															
Alt. 2	3	4												0	1	2					
TIMER 3												1	0								
Alt. 2									1	0											
TIMER 4															1	0					
Alt. 2																		1			0
32-kHz XOSC																	Q1	Q2			
DEBUG																			DC	DD	
OBSSEL											5	4	3	2	1	0					

Figure 5.3 Peripheral I/O pin Mapping [9]

three different input methods: Analog-to-Digital Converter (ADC), Universal Asynchronous Receiver Transmitter (UART) and Serial Peripheral Interface (SPI). The ADC is used to connect the analog sensor.

In this project, certain sensors are connected to the MCU in order to collect data from the miner and the environment. In order ensure all sensors are working, a program must be generated that connects each sensor to the correct pin in the hardware.

From the Figure 5.4, it can be observed that different ports in the development board have different names. In order to connect the sensors to their respective port, as in Figure 5.4, the table contained in Figure 5.3 and Table 5.1 should both be considered. For example, A7 is chosen as the input port. From the table in Figure 5.3, it can be discerned that A7 refers to pin P0.7. Subsequently, according to Table 5.1, the P0.7 pin refers to EM_P1_17 in the hardware. Depending on Figure 5.4, the position of the EM_P1_17 can be found in the development board. The sensor can then be connected to the MCU A7 port.

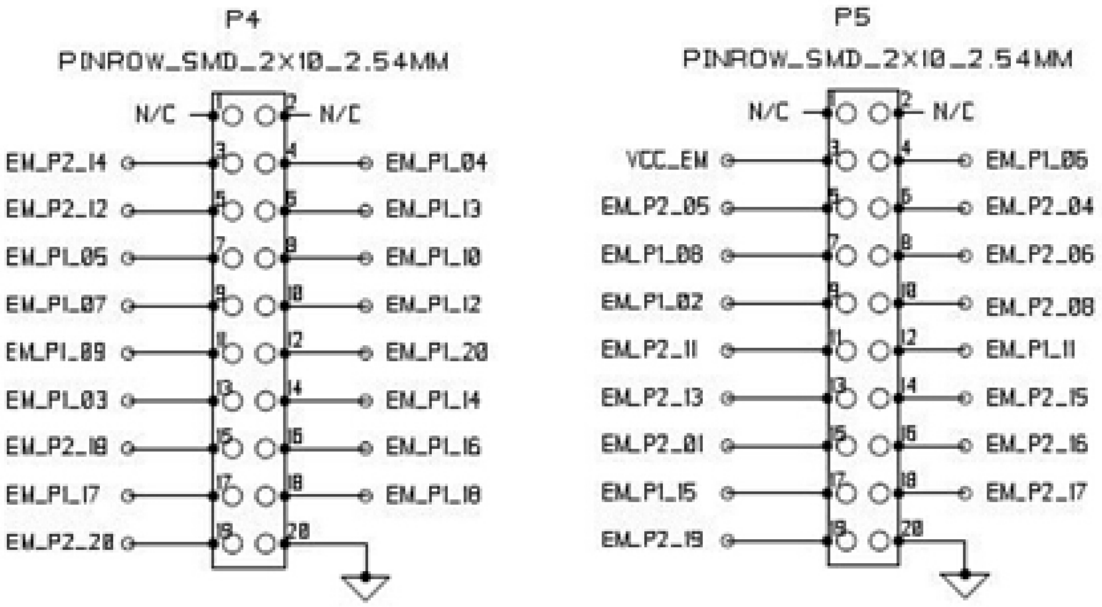

Figure 5.4 Hardware pins in development board [2]

Table 5.1 Connection between SOC port and development board port [2]

SOC	EM connect	SOC	EM connect
P0.0	EM_P1_11	P1.0	EM_P1_06
P0.1	EM_P1_05	P1.1	EM_P2_15
P0.2	EM_P1_07	P1.2	EM_P2_17
P0.3	EM_P1_09	P1.3	EM_P1_04
P0.4	EM_P1_03	P1.4	EM_P1_14
P0.5	EM_P2_18	P1.5	EM_P1_16
P0.6	EM_P1_15	P1.6	EM_P1_18
P0.7	EM_P1_17	P1.7	EM_P1_20

5.2 Temperature Sensor

The port AIN0-AIN7 can be utilized as the ADC (Analog-to-Digital Converter) input. The temperature sensor in the MCU can also be used as the ADC input for the temperature measurement. Registers TR0.ADCTM and ATEST.ATESTCTRL should be set for different situations.

The temperature sensor is an on-chip sensor in the CC2530. The sensor can be used to measure the temperature of the environment. The maximum value is 100 degrees and the minimum value is 0 degree. This sensor is an analog sensor in the MCU, which is connected to the channel 'ADC_TEMP_SENS'. The address of this channel is 0x0E. The measurement of the sensor is written in hexadecimal form. The sensor can be used to measure the temperature of the environment. The maximum value is 100 degrees and the minimum value is 0 degree.

The data collected from the ADC is not readable, and furthermore, must be translated to normal values. In order to develop an equation to compute the temperature, we must understand the rules of the in-build sensor. After conducting several experiments, the following rules can be drawn:

- When the temperature is 25 degrees, the value of the ADC is 1480.
- The value of the ADC changes by 4.5, while the temperature around the temperature sensor changes by 1 degree.

With the rules above, it can be derived that:

$$\begin{aligned} T_{real\,temperature} =& \frac{(V_{ADC} - (1480 - 4.5 \times 25))}{4.5} \\ =& \frac{(V_{ADC} - 1367.5)}{4.5}; \end{aligned} \tag{5.1}$$

In the IAR code, we can write:

```
#define VOLTAGE_AT_TEMP_25        1480
#define TEMP_COEFFICIENT          4.5


// Calibrate for 22C the first time the temp sensor
```

```
//is read.
// This will assume that the demo is started up in
//temperature of 22C
if(bCalibrate)
{
  voltageAtTemp22=value;
  bCalibrate=0;
}

temp = 22+((value - voltageAtTemp22)/TEMP_COEFFICIENT);

// Set 0C as minimum temperature, and 100C as max
if( temp >= 100)
{
  return 100;
}
else if (temp <= 0)
{
  return 0;
}
else
{
  return temp;
}
```

After the MCU is programmed, an experiment is conducted to analyze the result. In the experiment, a thermometer is employed to read the real temperature. The measured real temperature is compared with the read data in MCU. Different temperatures are measured in this experiment.

Table 5.2 outlines the real and computed temperatures in the experiment. From the Table 5.2, it can be discerned that the average error is within 1.5 degrees. For the environmental

Table 5.2 Comparisons between the real temperature and the measured temperature

	1	2	3	4	5
Measured temperature (degree)	8.2	10.4	15.8	20.5	29.5
Read data in MCU (degree)	6.8	9.8	13.9	19.2	28.1
Difference (degree)	1.4	0.6	1.9	1.3	1.4

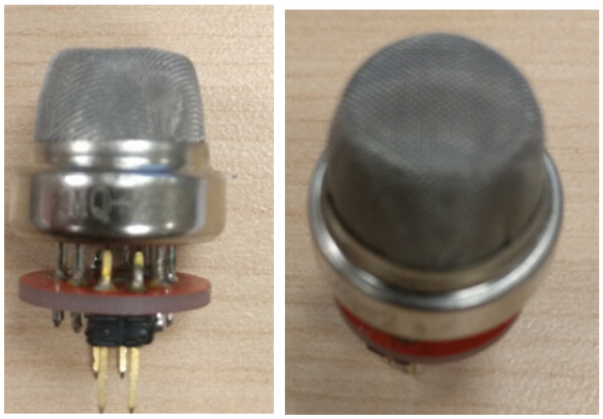

Figure 5.5 The appearance MQ-2

temperature, this error is acceptable.

5.3 Smoke detector

Harmful gas and fire are elements of danger to miners. A gas sensor known as MQ-2 is used to detect the smoke in this project. The appearance of MQ-2 can be observed in Figure 5.5. The MQ-2 is widely applied in both everyday use and in the industry. Normally, it can be used to detect smoke, hydrogen, alcohol, propane, i-butane, LPG and methane. The MQ-2 can also be referred to as a combustible-gas detector. The MQ-2 has a long and stable life, high sensitivity and an easy drive circuit. The sensitivity characteristic of the MQ-2 is the sensing resistance, which is denoted R_S. When the density of the smoke increases, the R_S decreases. Prior to using the sensor, it should be warmed up for an adequate amount of time. Otherwise, the output voltage and current will not yield accurate results. The range

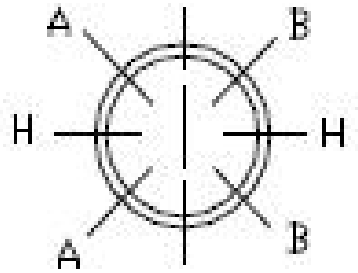

Figure 5.6 Pins of MQ-2 [10]

Figure 5.7 MQ-2 on the PCB board

of detecting smoke is between 100 to 10000 ppm ($1ppm = \frac{1cm^3}{1m^3} = 10^{-6}$).

The MQ-2 contains 6 pins. It can be deduced from Figure 5.6 that there are two 'H' pins, two 'A' pins and two 'B' pins. The 'H' pins are used to heat the sensor, while the 'A' pins and 'B' pins are used as input or output.

The MQ-2 is soldered to the sensor PCB, rendering it easier to connect to the MCU. As it depicted in Figure 5.7, there are 4 pins in the PCB: A1, B1, H1 and GND.

In order to use the sensor, a drive circuit is built which is contingent upon the requirements of the data sheet. Figure 5.8 illustrates the drive circuit.

From Figure 5.8, it can be deduced that the output voltage can be calculated as:

$$V_{out} = \frac{R_L}{R_L + R_S} \times V_{CC}; \tag{5.2}$$

Then the resistance of the MQ-2 sensor (R_S) can be calculated with:

$$R_S = (\frac{V_{CC}}{V_L} - 1) \times R_L; \tag{5.3}$$

The value of road resistance (R_L) in Table 5.3 is not fixed. The R_S represents the sensitive

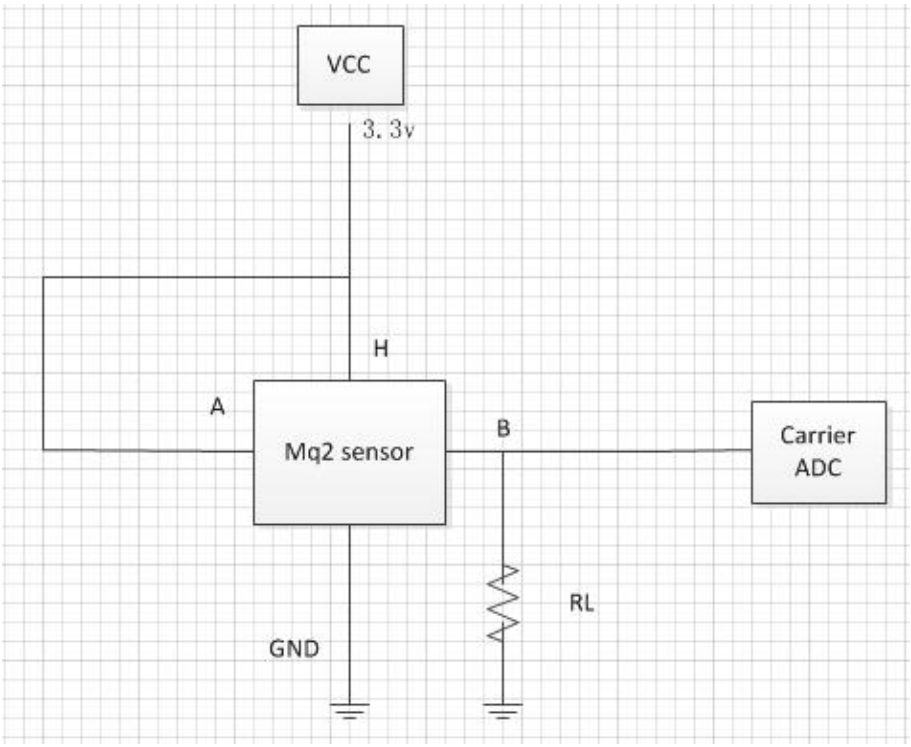

Figure 5.8 Drive circuit

resistance of the MQ-2, and will correspondingly decrease when the gas density increases, which signifies that the output voltage will similarly increase.

5.3.1 MQ-2 Static Calibration

In the event that there is no smoke and butane, the MQ-2 works in a static situation. As the request from the data sheet, when the sensor is in a static situation, the voltage in point B should be kept from 0.3 volts to 1 volt. Therefore, many road resistances are tested and an optimal one, with a static voltage between 0.3 and 1 volt, is selected for the system.

When conducting the tests, the MQ-2 sensor is located in pure air. After 2 minutes of pre-heating, the voltage in point B (V_L) is measured by the multimeter and recorded in Table 5.4.

From Table 5.4, it can be deduced that the most suitable road resistance is 0.984 $k\Omega$. Subsequently, the resistor value of 0.984 $k\Omega$ is chosen as the road resistance for the system. With this resistor, 6 sets of V_L are measured by multimeter and recorded in Table 5.5. From the Table 5.5, it can be discerned that the static voltage of the MQ-2 is approximately 0.54 V.

Table 5.3 The parameters of the drive circuit

Parameter Name	Technical Parameter
V_{CC}	Heating power: 3.3 Volts
MQ-2 sensor	MQ-2 smoke detector
R_S	The resistance of the MQ-2 sensor
Carrier ADC	ADC input in CC2530
A	Input pin
B	Output pin
H	Heating pin
R_L	Road resistance (not a fixed value)
GND	Ground: 0 Volts
Environmental temperature	23 degree

Table 5.4 MQ-2 static calibration for different resisters

Resister (Ω)	0	0.984k	17.8k	332.6k
Voltage (Volt)	0	0.546	2.165	2.386

Table 5.5 MQ-2 static calibration for resister 0.984kΩ

Time	1	2	3	4	5	6	Average
Voltage (Volt)	0.546	0.534	0.559	0.547	0.521	0.535	0.54

The resistance of the MQ-2 sensor in the static situation can be calculated with:

$$R_S = ((\frac{V_{CC}}{V_L}) - 1) \times R_L = ((\frac{3.3}{0.54}) - 1) \times 0.984k\Omega = 5.03k\Omega. \quad (5.4)$$

5.3.2 MQ-2 Dynamic Calibration

In the event that there is smoke or butane around the sensor, the MQ-2 works in a dynamic situation. The dynamic calibration is predominantly used to test the effect of the distance (density of smoke) on the output voltage (V_L).

As we know, the further away the MQ-2 sensor is from the fire point, the smaller the smoke density. This purpose of this section is to evaluate this theory. Two gases are used to test the MQ-2 sensor: smoke and butane. The smoke is made with burned paper, while the butane is made with a lighter.

The procedure of the experiment can be conducted with the following steps:

Step 1: Connect the circuit as depicted in Figure 5.8. Connect the circuit to the power supply and MCU.

Step 2: Pre-heat the MQ-2 sensor for approximately 2 minutes. Ensure that the sensor is fully heated (the sensor may be hot, which is a normal phenomenon).

Step 3: Use the static calibration to measure the static voltage of the sensor. Then, calculate the R_S.

Step 4: Prepare different scenarios and measure the output voltages using multimeter in point B in Figure 5.8. Record the results.

Four experiments are conducted to achieve the dynamic calibration. The smoke and the butane are tested separately with different distances. The results of the four experiments are introduced in the following four sections.

Experiment 1: Smoke from 30cm

The smoke is made with burned paper, and the paper is located 30cm away from the MQ-2 sensor. The output voltage is measured in point B. The results are recorded in Table 5.6.

The average of these 7 sets of data is 1.501 volts.

Table 5.6 The measurement of V_L with smoke from 30cm away

Times	1	2	3	4	5	6	7
Voltage (Volt)	1.511	1.521	1.487	1.485	1.475	1.528	1.501

Table 5.7 The measurement of V_L with smoke from 100cm away

Times	1	2	3	4	5	6	7
Voltage (Volt)	1.121	1.023	1.156	1.111	1.109	1.132	1.122

Experiment 2: Smoke from 100cm

The smoke is made with burned paper, and the paper is located 100cm away from the MQ-2 sensor. The output voltage is measured in point B. The results are recorded in Table 5.7.

The average of these 7 sets of data is 1.111 volts.

From Experiment 1, it can be discerned that the voltage increases from 0.54V to 1.501V. The difference is 0.961V. From Experiment 2, it can be discerned that ehe voltage increases from 0.54V to 1.111V. The difference is 0.571V. In these two experiments, the voltage difference changes from 0.961V to 0.571V when the burned paper moves from 30cm to 100cm.

Experiment 3: Butane from 30cm

The butane is made from a lighter and the lighter is located 30cm away from the MQ-2 sensor. The output voltage is measured in point B. The results are recorded in Table 5.8.

The average voltage of these 7 results is 3.052 volts.

Experiment 4:Butane from 100cm

The butane is made with a lighter and the lighter is located 100cm away from the MQ-2 sensor. The output voltage is measured in point B. The results are recorded in Table 5.9.

The average voltage of these 7 sets of data is 2.511 volts.

From Experiment 3, it can be discerned that the voltage increases from 0.54V to 3.052V. The difference is 2.512V. From Experiment 4, it can be discerned that the voltage increases

Table 5.8 The measurement of V_L with butane from 30cm away

Times	1	2	3	4	5	6	7
Voltage (Volt)	3.156	3.231	3.198	3.274	3.101	3.193	3.212

Table 5.9 The measurement of V_L with butane from 100cm away

Times	1	2	3	4	5	6	7
Voltage (Volt)	2.563	2.521	2.452	2.431	2.588	2.501	2.521

Table 5.10 Comparison between the voltages of the two gases in two distances

	Static Voltage	30cm	100cm
Smoke	0.54V	1.501V	1.111V
Butane	0.54V	3.052V	2.511V

from 0.54V to 2.511V. The difference is 1.971V. In these two experiments, the voltage difference changes from 2.512V to 1.971V when the burned paper moves from 30cm to 100cm.

The comparison is outlined in Table 5.10.

From the Table 5.10, it can be deduced that the voltage changes less when the distance is larger. It is imperative to set a suitable threshold value. The threshold value is set depending on how far away the fire should be detected. From the previous study, the distance can be set as 30cm. The threshold values for the two gases can be set as in Table 5.11.

5.3.3 Connect the MQ-2 Sensor to MCU

The experiments above were conducted to determine the calibration of the MQ-2 sensor. In the order to apply the sensor to this project, a connection between the sensor and MCU is necessary.

Port A0 is selected to connect the MQ-2 sensor. From the table in Figure 5.3, it can be deduced that Port A0 points to P0.0. With reference to Table 5.1, it can be deduced that the EM_P1_11 in the development board connects to P0.0 in the MCU. Figure 5.9 demonstrates the manner in which the sensors are connected to the MCU.

A driver should be coded with IAR to drive the ADC, as signified below:

```
int16 adcSampleSingle(uint8 reference,
```

Table 5.11 Threshold voltages for smoke and butane

	Static Voltage	Threshold Value
Smoke	0.54V	1.5V
Butane	0.54V	3.0V

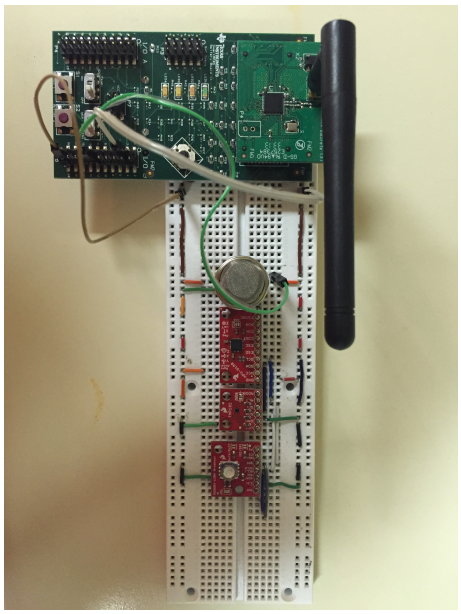

Figure 5.9 Development of the proposed sensor system

```
    uint8 resolution, uint8 channel)
{
    int16 value=0;

    ADC_ENABLE_CHANNEL(channel);

    ADCIF = 0;
    ADC_SINGLE_CONVERSION(reference |resolution |channel);
    while(!ADCIF);

    value  = (ADCH << 8) & 0xff00;
    value |= ADCL;
      /* Treat small negative as 0 */
 if (value < 0)
   value = 0;
  ADC_DISABLE_CHANNEL(channel);
    return value;
```

Table 5.12 The data read from MCU for the smoke experiment

Times	1	2	3	4	5	6	7
Static Voltage (Volt)	0.546	0.534	0.559	0.547	0.521	0.535	0.568
Dynamic Voltage (Volt)	3.156	3.231	3.198	3.274	3.101	3.193	3.212
Static read in ADC	3A	3A	39	3B	39	38	3A
Dynamic read in ADC	55	53	55	56	55	56	57

Table 5.13 The data read from MCU for the butane experiment

Times	1	2	3	4	5	6	7
Static Voltage (Volt)	0.546	0.534	0.559	0.547	0.521	0.535	0.568
Dynamic Voltage (Volt)	1.511	1.521	1.487	1.485	1.475	1.528	1.501
Static read in ADC	3A	3A	39	3B	39	38	3A
Dynamic read in ADC	88	89	87	88	87	88	8A

```
}
```

Subsequently, a function can be written in the main function::

```
 static uint8 readadc0(void)
{
  int16 adc0;
  uint8 adc1;
  adc0=adcSampleSingle(ADC_REF_AVDD, ADC_7_BIT, ADC_AIN0);
  adc1=(adc0&0x7f00)>>8;
  return adc1;
}
```

This function can enable the MCU to read the data from the MQ-2 sensor. All data from the senor is in hexadecimal form. For example, the data in the smoke experiment and the butane experiment can be read from the MCU as depicted in Table 5.12 and 5.13.

From Table 5.12 and Table 5.13, the static value and threshold value for smoke and butane can be rewritten in Table 5.14.

The static and threshold value can be set in MCU as outlined in Table 5.14. In normal time (no smoke and no butane), the value of the MQ-2 sensor should theoretically be the

Table 5.14 Threshold data in MCU for smoke and butane

	Static Value in ADC	Threshold Value in ADC
Smoke	3A	55
Butane	3A	87

static value. If the value of the MQ-2 is higher than the threshold, this signifies that a gas explosion is occurring. A warning must be given which indicates that the miner must keep away from said area.

6. Conclusion and Discussion

Mines represent a precious wealth of nature. Many countries devote copious amounts of time and resources into the mining industry. As the volume increases, more mining accidents are bound to occur. Many people die in these accidents, both in developed countries and developing countries. The ability to locate miners after an accident has occurred is indispensable to saving their lives. It is important to detect the dangers around the miners in advance in order for these miners to protect themselves. With this in mind, we developed a smart tracking system, which is designed to localize the miner, monitor the health of the miner and detect the surrounding environment.

This smart tracking system can be divided into three main components: the wearable device, transfer node and master control room. The wearable device is carried by the miner when he or she is performing a mining job. The transfer nodes are essentially installed on the wall. The Zigbee protocol is used to conduct the tracking and data transmission. The master control room is designed to deal with the collected information and, in turn, provide the relevant instructions.

The project is completed in four steps, the first step of which is to find an efficient way for the distance measurement. Finding a facile and accurate way to measure distance is important for localization. In this step, a 2-point localization method is developed using RSSI and Zigbee. The error is minimized using Gaussian distribution, statistical average and pre-setting points. By testing the designed 2-point localization method, a more optimal result is obtained, as compared to the existed model.

The second step is to improve the 2-point localization method developed in the first step. An improved method using three points to localize is developed in this step. In contrast to the existing localization method with three points, the improved method combines the 2-point

localization method and performs three computations in order to obtain an average. The accuracy is improved from 1.3412 meters (the accuracy of the 2-point localization method) to 0.6694 meters (the accuracy of the improved 2-point localization method).

Step three introduces the CC2530 development board and sensors, which are used in the system. Sensors are installed on the development board in order to render the wearable device multifunctional. The temperature sensor can help to measure the temperature of the environment. The MQ-2 sensor can detect different gases and smoke in the environment. In this project, smoke and butane are detected. According to the experiments, the thresholds of the amount of smoke and butane in the air are also set. The thresholds can enable the master control room to determine the areas of danger.

The final step predominantly discusses the transmission method for this project. The Zigbee protocol is used, as it has many advantages. The device can connect to a maximum of 65000 nodes, which is suitable for application in the mines, where thousands of miners are able to utilize the system simultaneously. The power supply is only 1mW for each unit. In the underground mine, the transfer node is used to receive the data package from wearable devices and transmit to the central computer. There are two situations for this step. If the data package is from the wearable device, the transfer node will measure the RSSI and create a new package which includes the data from the wearable device. Then, it transfers the new data package to the previous transfer node. If the data package is from the next transfer node, this transfer node will merely transfer the entire data package to the previous one. Using this method, the miner does not require any cables to connect transfer nodes. In the final transfer node, a data connection is installed, which is able to collect the data from the transfer node and transfer the data to the central computer using a serial cable. Finally, the master control room on the ground is able to track each miner underground and detect the dangerous regions.

6.1 Future Work

The project still has some room for improvement.

- Some noise is apparent when the transfer node measures the RSSI. A signal filter can be installed in the system which filters the noise in order to obtain a better result.

- More sensors can be installed in the device. In this project, the device is able to detect different gases and smoke. If more sensors are installed in the device, the miners and the master control room will be able to obtain more information from the data packages, and in turn, more optimal protection can be procured.

- The two-way communication can be further developed. In the project, the master control room on the ground can easily obtain the information underground. However, if the master control room intends to pass along messages to the miners or if one miner intends to talk to another miner, inter-phones may be required. Therefore, for further development, the function of the inter-phone can be added to the current system and then the communication will be upgraded to a two-way communication.

- A backup method should theoretically be developed, in the event that accident occurs. Furthermore, when an accident occurs, the master control room would be able to recognize the approximate position of each miner according to the last record. However, after the disaster occurs, the tunnel may be destroyed and the communication system may be ruined, culminating in a plethora of difficulties for message exchange between miners and the master control room. In the future, it would be prudent to develop a backup communication system.

References

[1] Y. Gu, A. Lo, and I. Niemegeers, "A survey of indoor positioning systems for wireless personal networks," *IEEE Communications Surveys Tutorials*, vol. 11, pp. 13–32, First 2009.

[2] Texas-Instruction, "CC2530 ZigBee Development Kit User's Guide," p. 41, April 2011.

[3] J. Mi and Y. Takahashi, "Low cost design of hf-band rfid system for mobile robot self-localization based on multiple readers and tags," in *2015 IEEE International Conference on Robotics and Biomimetics (ROBIO)*, pp. 194–199, Dec 2015.

[4] T. Novak, D. P. Snyder, and J. L. Kohler, "Post-accident mine communications and tracking systems," in *Industry Applications Society Annual Meeting, 2009. IAS 2009. IEEE*, pp. 1–8, Oct 2009.

[5] X. io Technologies, "x-IMU User Manual 5.2," November 2013.

[6] A. C. Berry, "The accuracy of the Gaussian approximation to the sum of independent variates," p. 49, 1941.

[7] Texas-Instruction, "CC253x Development Kit User's Guide," p. 1, April 2010.

[8] Texas-Instruction, "CC253x System-on-Chip Solution for 2.4-GHz User's Guide," *IEEE 802.15.4 and Zigbee Applications*, p. 18, April 2014.

[9] Texas-Instruction, "CC253x System-on-Chip Solution for 2.4-GHz User's Guide," *IEEE 802.15.4 and Zigbee Applications*, p. 81, April 2014.

[10] "Technical Data," *MQ-2 Gas Sensor*. Available at: `http://www.hwsensor.com`.

[11] A. K. John Sandlos, "Coal Ming," Mar 2015. Available at: `http://www.thecanadianencyclopedia.ca/en/article/coal-mining/`.

[12] "State Administration of Coal Mine Safety," in *National coal-mining safety accident report in China*, 2015. Available at: `http://www.chinasafety.gov.cn`.

[13] U.-S.-D. of Labor, "Mine Safety and Health Administration-MSHA," Mar 2015. Available at: http://www.msha.gov/newsinfo/2015/0326-coal-act/.

[14] M. Bender, "American law of mining," in *Rocky Mountain Mineral Law Foundation*, 1989.

[15] J. Caldwell, "Health and Safety," Dec 2015. Available at: http://technology.infomine.com/reviews/HAS/welcome.asp?view=full.

[16] C. F. Perucca, "Potash processing in Saskatchewana review of process technologies," *CIM bulletin*, pp. 61–65, 2003.

[17] F. J. Bellido-Outeirino, J. M. Flores-Arias, F. Domingo-Perez, A. G. de Castro, and A. Moreno-Munoz, "Building lighting automation through the integration of dali with wireless sensor networks," *IEEE Transactions on Consumer Electronics*, vol. 58, pp. 47–52, February 2012.

[18] S. Holm, "Ultrasound positioning based on time-of-flight and signal strength," in *Indoor Positioning and Indoor Navigation (IPIN), 2012 International Conference on*, pp. 1–6, Nov 2012.

[19] C. Takahashi and K. Kondo, "Indoor positioning method for augmented audio reality navigation systems using ibeacons," in *2015 IEEE 4th Global Conference on Consumer Electronics (GCCE)*, pp. 451–452, Oct 2015.

[20] MINETEC, "Smarts," 2015. Available at: http://www.minetec.com.au/our-solutions/productivity/smarts/.

[21] C. Zhou, J. Downey, D. Stancil, and T. Mukherjee, "A low-power shoe-embedded radar for aiding pedestrian inertial navigation," *IEEE Transactions on Microwave Theory and Techniques*, vol. 58, pp. 2521–2528, Oct 2010.

[22] T. Willemsen, F. Keller, S. Lorey, and H. Sternberg, "Museum of the moment: A cooperation project between metropolitan culture and geomatics," in *Indoor Positioning*

and Indoor Navigation (IPIN), 2014 International Conference on, pp. 375–384, Oct 2014.

[23] W. Ming-Xiao, Z. Tao, X. Miao-Rong, Z. Bin, and J. Ming-Qiu, "Analysis Of National Coal-mining Accident Data In China, 2001-2008," *Public Health Reports*, vol. 126, no. 2, pp. 270–275, 2011.

[24] G. P. Yost and S. Panchapakesan, "Improvement in estimation of time of arrival (toa) from timing advance (ta)," in *Universal Personal Communications, 1998. ICUPC '98. IEEE 1998 International Conference on*, vol. 2, pp. 1367–1372 vol.2, Oct 1998.

[25] H. Tian, S. Wang, and H. Xie, "Localization using cooperative aoa approach," in *2007 International Conference on Wireless Communications, Networking and Mobile Computing*, pp. 2416–2419, Sept 2007.

[26] T. Alhmiedat, F. Omar, and A. A. Taleb, "A hybrid tracking system for zigbee wsns," in *Computer Science and Information Technology (CSIT), 2014 6th International Conference on*, pp. 71–74, March 2014.

[27] G. R. Allcock, "The time of arrival in quantum mechanics i. formal considerations," *Annals of physics*, vol. 53, no. 2, pp. 253–285, 1969.

[28] "CC2530: Second Generation System-on-Chip Solution for 2.4 GHz IEEE 802.15.4 / RF4CE / ZigBee," Dec 2014. Available at: Texas Instruments Incorporated, `http://www.ti.com/product/CC2530`.

[29] R. Zemek, S. Hara, K. Yanagihara, and K. Kitayama, "A Traffic Reduction Method for Centralized RSSI-Based Location Estimation in Wireless Sensor Networks," *IEICE TRANSACTIONS ON COMMUNICATIONS*, pp. 1842–1851, May 2008.

[30] X. Zhang, R. Shrestha, and K. A. Wahid, "An efficient algorithm for localization using RSSI based on zigbee," in *IEEE 28th Canadian Conference on Electrical and Computer Engineering, CCECE 2015, Halifax, NS, Canada, May 3-6, 2015*, pp. 366–369, 2015.

[31] Z. Jianyong, L. Haiyong, C. Zili, and L. Zhaohui, "Rssi based bluetooth low energy indoor positioning," in *Indoor Positioning and Indoor Navigation (IPIN), 2014 International Conference on*, pp. 526–533, Oct 2014.

[32] J. Aldrich and J. Miller, "Earliest uses of symbols in probability and statistics," *Electronic Document, retrieved March*, vol. 20, 2005.

[33] Z. Jianwu and Z. Lu, "Research on distance measurement based on rssi of zigbee," in *Computing, Communication, Control, and Management, 2009. CCCM 2009. ISECS International Colloquium on*, vol. 3, pp. 210–212, Aug 2009.

[34] Z. Jianwu and Z. Lu, "Research on distance measurement based on rssi of zigbee," in *2009 ISECS International Colloquium on Computing, Communication, Control, and Management*, vol. 3, pp. 210–212, Aug 2009.

[35] T. Elarabi, V. Deep, and C. K. Rai, "Design and simulation of state-of-art zigbee transmitter for iot wireless devices," in *2015 IEEE International Symposium on Signal Processing and Information Technology (ISSPIT)*, pp. 297–300, Dec 2015.

[36] Bluetooth-SIG-Inc., "Bluetooth technology basics," May 2016. Available at: `https://www.bluetooth.com/what-is-bluetooth-technology/bluetooth`.

[37] "Low energy," Dec 2014. Available at: Bluetooth SIG Inc., `http://www.bluetooth.com/Pages/low-energy-tech-info.aspx`.

[38] A. Balasubramanian, R. Mahajan, and A. Venkataramani, "Augmenting mobile 3g using wifi," in *Proceedings of the 8th international conference on Mobile systems, applications, and services*, pp. 209–222, ACM, 2010.

[39] "Embedded Security-BodyCom Technology," Dec 2014. Available at: Microchip Technology Inc., `http://www.microchip.com/pagehandler/en-us/technology/embeddedsecurity/technology/bodycom.html`.

[40] M. C. Lin, F. Y. Huang, and T. D. Chiueh, "A-nfc: Two-way near-field communications (nfc) via inaudible acoustics," in *Information, Intelligence, Systems and Applications (IISA), 2015 6th International Conference on*, pp. 1–6, July 2015.

[41] J. Liu, X. Tan, and H. Min, "Dual frequency based real time location system using passive uhf rfid," in *ASIC (ASICON), 2011 IEEE 9th International Conference on*, pp. 779–782, Oct 2011.

[42] R. Mautz, "Indoor Positioning Technologies," p. 91, Feb 2012.